공학박사 학위논문

Development of Magnet System for Electron Paramagnetic Resonance Tooth Dosimetry and Application to in-vivo Assessment

전자상자성공명 치아 누적 방사선량 측정을 위한 자석 개발 및 체내 선량평가에의 적용

2022년 8월

서울대학교 융합과학기술대학원
융합과학부 방사선융합의생명전공

최 권

A Dissertation for the Degree Doctor of Engineering

Development of Magnet System for Electron Paramagnetic Resonance Tooth Dosimetry and Application to in-vivo Assessment

전자상자성공명 치아 누적 방사선량 측정을 위한 자석 개발 및 체내 선량평가에의 적용

August 2022

Program in Biomedical Radiation Science
Department of Transdisciplinary Studies
Graduate School of Convergence Science and Technology

Kwon Choi

Development of Magnet System for Electron Paramagnetic Resonance Tooth Dosimetry and Application to in-vivo Assessment

지도 교수 예성준

이 논문을 공학박사 학위논문으로 제출함

2022년 8월

서울대학교 융합과학기술대학원
융합과학부 방사선융합의생명전공

최 권

최권의 공학박사 학위논문을 인준함
2022년 8월

위 원 장	김 현 진	(인)
부위원장	예 성 준	(인)
위 원	최 희 동	(인)
위 원	김 인 중	(인)
위 원	Hiroshi Hirata	(인)

Development of Magnet System for Electron Paramagnetic Resonance Tooth Dosimetry and Application to in-vivo Assessment

Sung-Joon Ye

Submitting a Ph.D. Dissertation of Engineering

Aug 2022

Graduate School of Convergence Science and Technology
Seoul National University
Program in Biomedical Radiation Sciences

Kwon Choi

Confirming the Ph.D. Dissertation written by Kwon Choi
Aug 2022

Chair	Hyeon Jin Kim	(인)
Vice Chair	Sung-Joon Ye	(인)
Examiner	Hee Dong Choi	(인)
Examiner	In Jung Kim	(인)
Examiner	Hiroshi Hirata	(인)

Abstract

Keyword : Electron paramagnetic resonance, In vivo dosimetry, EPR tooth dosimetry, Pseudo-in-vivo phantom, Q factor variable, Total body irradiation
Student Number : 2012-23872

For the triage purpose in the large radiation accident situation, the in vivo electron paramagnetic resonance (EPR) tooth dosimetry is a unique and useful tool. It can rapidly distinguish irradiated ones from others. For the counter accident, the mobility to move to the accident location is also an important factor. For this purpose, a new EPR magnet was developed with the lighter weight, and the in vivo optimized design in this thesis. This was also a part of the project to develop the entire EPR spectrometer comprehensively.

In the second part of the thesis, in vivo tooth dosimetry was described. Even with the dose-response curve acquired from extracted teeth, a dose-response data from in vivo measurements is required due to the different dosimetric sensitivity under in vivo circumstances, which is represented by Q factor. Also it was shown that there was difference in Q factor between individuals observed from volunteers' teeth in their oral cavity. To reflect the difference between individuals, a new method was suggested. The newly suggested pseudo-in-vivo phantom did an important role in this method. The Q factor could be intentionally changed in the range of in vivo measurements.

Throughout the thesis, the performance of the developed magnet was verified through three steps. First, the magnetic flux density was measured and compared with the finite element method (FEM) simulation. Second, EPR spectrum was acquired from irradiated teeth as the preliminary test. For this, two intact human incisors irradiated 5 and 30 Gy with 220 kVp X-ray were measured.

As the final test, EPR spectra was measured from post-radiotherapy patients and the tooth absorbed doses were assessed with in vivo measurement. For this, dose-response curves for various Q factors were acquired prior to the in vivo assessments. In the process to collect the dose-response data, the aforementioned pseudo-in-vivo phantom was used. Four intact human incisor teeth were used to collect the dose-response data. From the dose-response data, the Q factor relationships between the dosimetric sensitivity and background signal was acquired. From these relationships, a patient adopted dose-response curve was generated with a patient's specific Q factor. The irradiated doses were assessed from two post-TBI patients with this method. Based on the dose-response curves, the doses which the patients were irradiated during the treatments were estimated.

Contents

List of Tables

List of Figures

Chapter 1. Development of EPR Spectrometer

1. Basics of Electron Paramagnetic Resonance

1.1. Principle of Electron Paramagnetic Resonance

Electron paramagnetic resonance (EPR) is a resonance technique that studies energy differences in a sample with unpaired electrons. The magnetic properties of a material with unpaired electrons are mainly paramagnetic. The energy difference detected by EPR is predominately due to the interaction of the unpaired electrons in the sample with an external magnetic field, B_0.

When an external magnetic field is applied, the unpaired electrons align in the parallel or anti−parallel direction to B_0. This is called Zeeman splitting. These electrons are polarized with two different spin momenta, $m_s = +\frac{1}{2}$, or $m_s = -\frac{1}{2}$, along their aligned direction to B_0. Differences in spin momentum result in different energy states. The energy states of the electron can be calculated as $E = g_e \mu_B B_0 m_s$, and each state is

$$E_{+1/2} = \frac{1}{2} g_e \mu_B B_0 \tag{1}$$

$$E_{-1/2} = -\frac{1}{2} g_e \mu_B B_0 \tag{2}$$

where g_e is a g−factor of a free electron, which is 2.002319, and μ_B is the Bohr magneton, which is $9.2740100783 \times 10^{-24}\ J \cdot T^{-1}$. An electron with a direction against the magnetic field has a higher energy state because its direction is opposite to that of the proton. The energy difference between $E_{+1/2}$ and $E_{-1/2}$ is measurable by EPR when the required energy, $h\nu$, for the electrons to transition from one state to another is applied to the sample; this energy is equivalent to ΔE.

$$\Delta E = g_e \mu_B B_0 \Delta m_s = g_e \mu_B B_0 = h\nu \tag{3}$$

where h is the Planck constant $(= 6.62607015 \times 10^{-34} J \cdot Hz^{-1})$ and ν is the frequency of the applied microwave (Figure). Under the

condition $\Delta E = h\nu$, the unpaired electrons in the two states keep exchanging their energy states, absorbing or emitting energy, $h\nu$. By the Maxwell–Boltzmann distribution, there is a higher number of unpaired electrons in the lower energy state than in the higher one. This results in the net absorption of energy, which enables quantitative measurements of paramagnetic materials.

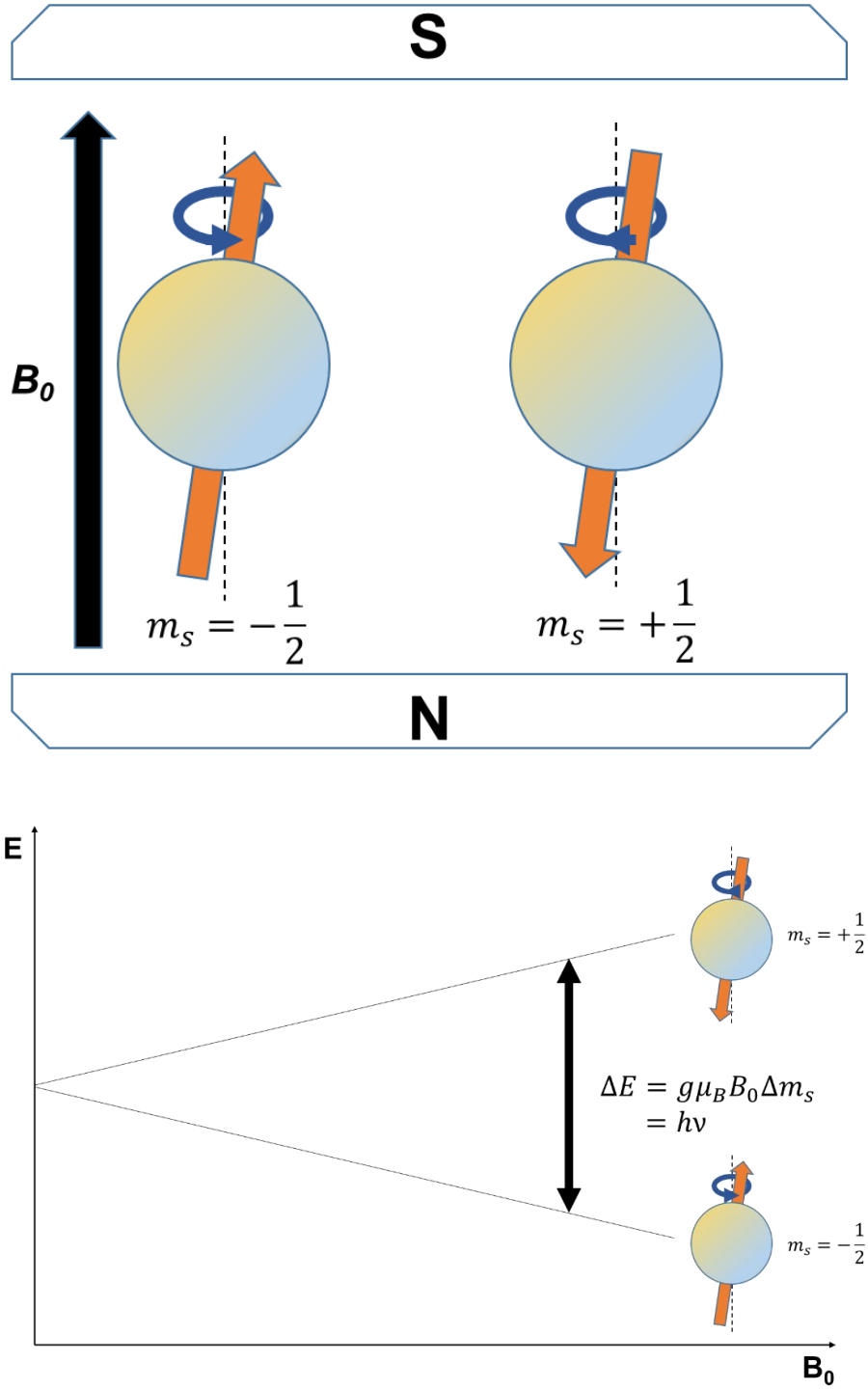

Figure 1 Theory of EPR measurement

1.2. Principle of Continuous Wave EPR Spectrometer

The resonance conditions for the measurement of the EPR signal is that the frequency, ν, matches the magnetic field, B_0 as shown in equation (3). Because the energy difference, ΔE, increases as B_0 becomes stronger, a higher frequency is required for the resonance. The required frequency is calculated as in equation (4):

$$\nu = \frac{g\mu_B B_0}{h} \tag{4}$$

From this relationship between the frequency and magnetic field, there are two ways to measure the EPR spectrum. One way is to change the frequency while keeping the strength of the magnetic field, B, constant; the spectrum is then acquired on the scanning range of frequency. In these spectra, the resonance peak appears when the changing frequency becomes ν, and equation (4) is satisfied. This method is technically difficult to be implemented.

Another method is through continuous wave (CW) EPR; this method is adopted in most spectrometers. Here, the spectrum is collected while changing the magnetic field and keeping the frequency at a constant value, which satisfies the resonance condition (4). To "sweep" or scan the range of the magnetic field around B_0, a sweep magnetic field is required to be operated separately from B_0. For this, the sweep magnetic field is generated by a separate electromagnet. The sweep magnetic field starts to apply the field in the opposite direction to B_0, and continuously increases its strength. The sweep ends when the direction of the sweep magnetic field is similar to that of B_0. B_0 is kept constant during this operation. This results in a magnetic field scanning range from $B_0 - B_{-sweep}$ to $B_0 - B_{+sweep}$.

In this scanning process, the g−factor is used to discriminate the characteristics of the materials evaluated in the EPR measurement.

$$g = \frac{h\nu}{\mu_B B_0} \tag{5}$$

The g−factor is a constant value, which is independent of ν or B_0. It characterizes the magnetic momentum of an atom, a particle, or the nucleus.

2. Development of in vivo EPR Spectrometer

2.1. Motivation of the Development

2.1.1. *In Vivo* Tooth Dosimetry

Large-scale radiation accidents such as the Chernobyl disaster or the Fukushima Daiichi accident have the potential to expose large populations to unexpected doses of radiation. Although thousands of victims are potentially exposed to the radiation, providing all the people with treatment for the most severe level of exposure is not feasible. Moreover, though severely exposed individuals urgently need proper management and treatment, persons that are irradiated but without clinical symptoms require no immediate treatment. Generally, 2 Gy is the threshold above which clinical symptoms occur for an exposed individual. Therefore, it can be inferred that the screening of individuals exposed to clinically meaningful doses from thousands of victims is important to effectively focus the available treatment on those in critical need. Particularly, in the triage of a large-scale of victims, screening is required to be sufficiently fast to achieve high throughput within a limited time and with limited manpower.

Although the gold standard for the radiation triage is the chromosome analysis, the assessment takes a long time and the discernment of skilled workers. This can be a limitation for a triage tool in the assessment of a large number of persons. Hence, for fast assessment, in vivo EPR tooth dosimetry has been proposed as a suitable option. It can measure and assess one subject in a few minutes with high throughput. It is relatively easily operated by less-skilled operators. Furthermore, in several previous studies, in vivo EPR devices had been developed in light and compact forms so that it could be directly carried in a vehicle to the location of the counter-accident. Moreover, in vivo EPR tooth dosimetry is a unique technique to measure human subjects noninvasively.

2.1.2. *Motivation of the Study*

In previous studies, our group developed the in vivo EPR spectrometer including a microwave bridge, resonator, and receiver part. However, the magnet adopted was from another group in Dartmouth College. For the full development of the device and further study in the field, it was necessary for the magnet to be studied thoroughly and potentially custom built.

Another reason for the development of the magnet is that in vivo EPR tooth dosimetry requires customization of the magnet for convenient measurements of the subjects.

After the development of the magnet, it should be utilized in actual in vivo studies. Therefore, Chapter 2 of this thesis presents the in vivo EPR tooth dosimetry.

The number of actual irradiated subjects is limited; hence, an alternative method was considered for the dose–response curve acquisition. The pseudo-in-vivo phantom was fabricated for this alternative method; the Q factor of the phantom was controlled to the level of the in vivo situation. The flexibility of the controlling Q factor is a novelty of our study. This is the first study to attempt the application of pre-obtained EPR dose–response curves to varying Q factor of subjects in vivo.

Based on the outcome of this study using the pseudo-in-vivo phantom, actual patients were measured in vivo and assessed for verification. The total body irradiation (TBI) patients were measured as subjects.

3. Development of the Magnet for in vivo EPR Spectroscopy

3.1. Motivation of the Development

The triage of a large population is a critical social demand when a nuclear accident occurs, such as the Chernobyl disaster in 1986 and the Fukushima Daiichi nuclear accident in 2011. While the number of potential patients is large, the individual radiation damage is widely distributed from a slight to life-threatening dose. Depending on the degree of significance, the proper management and treatment of injuries is urgently required [1]. Hence, a triage is needed to assess the radiation dose. Additionally, a quick assessment of the radiation dose for individuals is required to be performed on-site, but technologies for this are limited. The current gold standard for dose assessment in exposed individuals is a dicentric scoring analysis [2]. However, dicentric analysis is a laborious and time-consuming method that requires 72–96 h for lymphocyte culture and manual scoring by an expert. Even with advanced improvements, such as automated dicentric analysis takes 48 h only for cell culturing [3].

In vivo EPR tooth dosimetry is a currently available technique for noninvasive radiation dose assessment in human subjects. EPR is employed in radiation dosimetry by quantifying the amount of radicals generated by ionizing radiation [4]. Ionizing radiation generates stable CO_2^- radicals in calcified human tissues, such as the tooth enamel and bone. *In vivo* EPR tooth dosimetry is useful, especially in radiological accidents, where most potential victims do not possess appropriate dosimeters [5]. It can rapidly assess an exposure dose in 10 min, including 5 min of measurement and 5 min of assessment. These advantages have been exploited to estimate the exposure of victims retrospectively in radiation accidents [6-8].

In vivo EPR tooth dosimetry has been extensively studied [5, 9-11]. The *in vivo* method evaluates intact human teeth noninvasively without the requirement of preprocessing, on-site response, and expeditiousness during dose estimation. In conventional methods, a microwave frequency of 9 GHz or higher is

used, which is easily absorbed into aqueous material in the *in vivo* studies. Thus, most *in vivo* studies chose low frequencies of approximately 1 GHz to avoid the interference of water [5, 9]. The X-band frequency has been considered for *in vivo* tooth dosimetry alongside a modified X-band resonator [10, 11]. Owing to the lack of commercially available spectrometers for human studies, specific devices have to be developed for *in vivo* studies aiming at human applications. Hirata et al. [12] developed an electronically tunable resonator for *in vivo* EPR measurement. Guo et al. [10, 11] also developed a resonator to measure *in vivo* tooth dosimetry using the X-band.

Moreover, the *in vivo* method makes it relatively easy for unskilled workers to assess the radiation dose of an exposed person, making *in vivo* EPR tooth dosimetry suitable for an on-site patient triage tool. To deploy EPR-based dosimetry instruments to places close to a disaster area or shelters of evacuees, EPR instruments should be mobile and easily operated. However, the magnet of an EPR spectrometer and its power supply are generally heavy. This is an obstacle when transferring the EPR spectrometer from a laboratory to a field near a disaster area.

Using permanent magnet (PM) arrays reduces the weight of the magnet and is relatively inexpensive [13]. A car-mounted magnetic resonance imaging system for on-site diagnosis was proposed [14]. The magnet weighed 200 kg and was deployable using a car. Swartz et al. [15] developed a deployable EPR spectrometer for *in vivo* tooth dosimetry, including the magnet. The magnet weighed 30 kg [16]. Numerous studies on *in vivo* EPR dosimetry have been recently reviewed. Sato-Akaba et al. [17] used small neodymium magnet arrays to form a homogeneous magnetic field for biological EPR imaging. The magnet combined with coils weighed 6 kg. Sirota et al. developed a magnet for pulsed EPR tooth dosimetry by adopting the *ex situ* methodology of nuclear magnetic resonance (NMR) [18]. They also attempted *in vivo* tooth dosimetry with another type of magnet under an 11.2-GHz frequency [19].

In this study, we develop a magnet system using PMs with

deployable weight for *in vivo* EPR tooth dosimetry. The magnet system for *in vivo* EPR dosimetry is a key component to be developed by in-house users. Although there have been many studies that have developed a magnet system for general purposes, including NMR and magnetic hyperthermia, the number of EPR studies describing the development of magnet systems for *in vivo* tooth dosimetry is limited [20-22].

The development described in this study is part of the entire development of an *in vivo* EPR spectrometer for tooth dosimetry. In this study, a magnet system customized *in vivo* EPR tooth dosimetry was developed using PMs and copper coils. First, the design and fabrication of the magnet system are described. Subsequently, the performance of the magnet system is evaluated in terms of the magnetic flux density and uniformity. Finally, the *ex vivo* EPR spectra are measured to verify the magnet system' s performance.

3.2. Materials and Methods

3.2.1. Design Concept and Required Specifications

As mentioned above, we fabricated an EPR magnet with deployable weight for *in vivo* tooth dosimetry in this study. Therefore, the required specifications are determined from the viewpoint of the weight (deployability), pole gap width, main magnetic flux density, magnetic field homogeneity, sweep field width, and amplitude of the modulation field.

For the magnet to be deployable, at least by a car, it should be sufficiently light to be loaded onto a vehicle by one person. Based on the study by Williams et al. [16], the weight should be equal to or lower than 30 kg. The pole gap of the magnet was determined considering the subject' s head size. Because the subject' s head is located between the pole gap to measure the tooth *in vivo*, a sufficiently wide space should be considered between the two poles of the magnet. This would be 18 cm because of a statistical reason presented later in the description of the EPR magnet design.

Meanwhile, the main magnetic flux density, B_0, and homogeneity required for tooth dosimetry should be secured. The B_0 is determined based on the microwave frequency used for operation. A high frequency tends to be absorbed by tissues around the measured tooth. Therefore, frequencies of approximately 1.2 GHz have been adopted as the detection frequencies in several preclinical and clinical systems, compromising between the sensitivity and detection depth [9]. The required B_0 was calculated as 42.9 mT. The B_0 field should be sufficiently homogeneous over the sample volume [23]. The least required homogeneity of B_0 is determined by the variation of B_0 over the sample volume and linewidth of the evaluated sample. As a rule of thumb, the variation in the magnetic field strength over the sample should be less than 10% of the linewidth of the sample signal [23]. For the tooth dosimetry, the linewidth of the radiation-induced signal (RIS) of a tooth is known to be 0.26 mT [9, 24, 25] so that the required B_0

variation is 0.026 mT. The scannable range of the magnetic field should include the spectrum of the reference material, 4−oxo−2,2,6,6−tetramethylpiperidine−d_{16}−1−^{15}N−1−oxyl (^{15}N−perdeuterated tempone (^{15}N−PDT), CDN Isotopes, Quebec, Canada) and that of the tooth. The least sweep range required for this is approximately 3.5 mT. The amplitude of the RIS of the tooth EPR spectrum is known to be maximized at a 0.4−mT field modulation. In our design, a modulation field of 0.4 mT is planned for application in the tooth sample location. The modulation frequency should be more than 20 kHz, which is a limitation of the audible frequency due to its *in vivo* application.

3.2.2. EPR Magnet Configuration

Fig. 1 shows a schematic design of the EPR magnet system for *in vivo* tooth dosimetry. The magnet system typically comprises PMs, magnetic field sweep coils, and magnetic field modulation coils. PMs are used to generate the Zeeman magnetic field of the L-band (1.2 GHz in this study). In CW EPR, the spectrum is acquired by scanning magnetic fields around the main magnetic field (B_0). This spectrum is acquired in the presence of an alternating current (AC) magnetic field formed by the magnetic field modulation coils.

B_0 is generally provided by electromagnets in commercial EPR spectrometers using relatively higher frequencies, such as the X- or Q bands. PMs are also available in the applications of L-band or lower frequencies, which are broadly used for *in vivo* measurements. Adopting PMs for B_0 has an advantage over electromagnets by reducing the number of devices for electromagnet operation, such as a power supply and cooling system.

Each magnetic field sweep coil comprises two separate axially aligned identical circular coils operated with direct current (DC). By applying DC to the sweep coil, the main magnetic field varies in strength. Each magnetic field modulation coil also comprises two identical circular coils operated with AC.

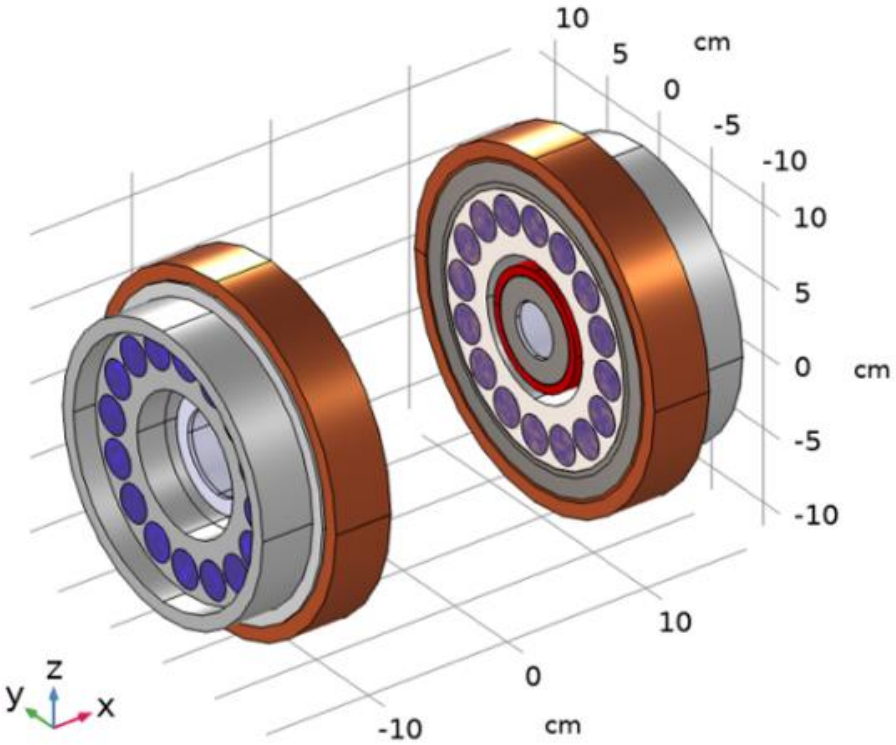

Figure 2 Schematic design of EPR magnet system for *in vivo* tooth dosimetry. The magnet system typically comprises PMs (blue), sweep (brown), and modulation coils (red). It should be noted that the direction of the main magnetic field is on the X axis.

3.2.3. EPR Magnet Design

B_0 is static and equivalent to the Zeeman magnetic field of the subject material under evaluation. Sintered $Nd_2Fe_{14}B$ (NdFeB) was adopted for the PM material. NdFeB is one of the strongest commercially available PM materials. Cylindrical PMs with a 2.5-cm diameter and 6.2-cm length were used. A total of 32 NdFeB cylindrical magnets were used to make two ring arrays, which were axially aligned (Blue in Fig. 1). Thus, 16 PMs were aligned in parallel in each ring. The magnetic flux density generated by the two PM ring arrays was measured at the center region of the two axially aligned rings, where a subject for the EPR measurement was positioned.

Between the two axially aligned ring arrays, the space where a subject' s head is located for *in vivo* tooth dosimetry should be considered. A homogeneous magnetic field region is formed around the center between the two ring arrays. For *in vivo* measurement, a homogeneous magnetic field should be formed, where the upper incisors are located when a subject' s head is positioned between the two poles of the magnet. Some studies statistically estimated the human head size of ethnic groups [26-28]. The head breadth is the maximum horizontal width of the head above the ears and is used to determine the pole gap. From the Civilian American and European Surface Anthropometry Resource (CAESAR) database of North Americans, the maximum head size was estimated to be 17.2 cm in both genders of Caucasian, African, Asian, and Hispanic subjects [28]. A pole gap of 18 cm would be enough to examine most people, although the top 5% of the male group was reported to have a head breadth of 18.2 cm in a study targeting Taiwanese. In this study, the actual gap width between the two PM ring arrays was set as 19 cm with a 0.5-cm thick lamination plate attached to the inner face of each pole.

The sweep coil has an inner and outer radius of 9.0 and 10.29 cm, respectively, with a width of 3.95 cm, which was placed on the

surroundings outside the PMs (Brown in Fig. 1). The EPR measurement for tooth dosimetry requires a sufficient magnetic sweep range to include the spectra combined with signals of the reference materials and tooth RIS. In this study, ^{15}N−PDT was used as a reference material, where the spectrum had two peaks sufficiently included within a 3.5−mT magnetic field sweep when using a 1.2−GHz frequency. To satisfy this requirement with a reasonably tolerable current, 100 turns were wound using a copper wire with a diamater of 2.2 mm on each side of the sweep coil. The gap between both sides of the coils was the same as that of the PMs. The number of turns and diameter of the coils were determined by the guidance of the finite element method (FEM) simulation presented below.

The magnetic field modulation coil operates at 21.2 kHz. The modulation coil has an inner and outer radius of 3.3 and 3.97 cm, respectively, with a width of 3.6 cm, which is placed inside the PM ring arrays (Red in Fig. 1). Eighty−two turns are wound using a copper wire with a diameter of 1.6−mm on each side. Owing to the characteristic of the AC magnetic field inducing eddy currents in the adjacent conductive materials, the parts nearby were built with nonconductive materials, except for the coils and PMs.

3.2.4. Analytical Calculation of Magnetic Flux Density of PMs

At the design stage, B_0 was calculated as 42.9 mT assuming ν = 1.2 GHz when g of the radiation-induced radical of tooth was approximately 2.0. Thus, the grade of the NdFeB magnet was determined to adjust B_0 close to 42.9 mT.

To adjust the central magnetic field to the Zeeman magnetic field, the magnetic field generated by the PMs was calculated. The central magnetic field was calculated as the sum of the magnetic fields of each PM. The remanent flux density, B_r, of the PM was determined as a nominal value of 1.31 T, which was close to the NdFeB grade of N42.

To adjust the central magnetic field to the Zeeman magnetic field, the magnetic field generated by the PMs was calculated. The central magnetic field is calculated from the sum of the magnetic fields from each PM. When each PM is magnetized in M_s in its axial direction, the magnetic field of one PM is given by

$$B(x) = \nabla \times A = \frac{\mu_0}{4\pi}\int \boldsymbol{j_m}(X') \times \frac{(X - X')}{|X - X'|^3} dv' \tag{6}$$

$$\boldsymbol{j_m} = \hat{\varphi}\boldsymbol{M_s} = \mathrm{M_s}[(-sin\varphi)\hat{x} + (cos\varphi)\hat{y}] \tag{7}$$

where $\boldsymbol{j_m}$ is the surface current density by magnetization, X is an arbitrary point where the magnetic field is calculated, X' is a point on the surface of the PM (Figure 3).

$$\vec{B} = \frac{\mu_0}{4\pi}\int M_s[(-sin\varphi)\hat{x} + (cos\varphi)\hat{y}] \times \frac{(a-cos\varphi)\hat{x}+(-R\,sin\varphi)\hat{y}+(b-z)\hat{z}}{[(a-cos\varphi)^2+(-R\,sin\varphi)^2+(b-z)^2]^{3/2}} ds$$

$$= \frac{\mu_0}{4\pi}\int M_s \frac{((b-z)\,cos\varphi)\hat{x} + ((b-z)\,sin\varphi)\hat{y} + (R\,sin2\varphi + R\,cos2\varphi - a\,cos\varphi)\hat{z}}{[(a-cos\varphi)^2 + (-R\,sin\varphi)^2 + (b-z)^2]^{3/2}} ds \tag{8}$$

$$= \frac{\mu_0}{4\pi}\int M_s \frac{(b-z)\hat{r} + (\varphi)\hat{\varphi} + (R\,sin2\varphi + R\,cos2\varphi - a\,cos\varphi)\hat{z}}{[(a-cos\varphi)^2 + (-R\,sin\varphi)^2 + (b-z)^2]^{3/2}} ds$$

In this study, only the magnetic field in the axial axis is considered, which is

$$\overrightarrow{B_z} = \frac{\mu_0}{4\pi}\int M_s \frac{R\,sin2\varphi + R\,cos2\varphi - a\,cos\varphi}{[(a-cos\varphi)^2 + (-R\,sin\varphi)^2 + (b-z)^2]^{3/2}}\,ds$$

$$= \frac{\mu_0\,M_s}{4\pi}\int_{-L}^{0}\int_{0}^{2\pi} \frac{R - a\,cos\varphi}{[(a-cos\varphi)^2 + (-R\,sin\varphi)^2 + (b-z)^2]^{3/2}}\,R\,d\varphi\,dz$$

$$= \frac{\mu_0\,M_s\,R}{4\pi}\int_{-L}^{0}\left[\left\{\frac{\sqrt{\frac{a^2-2aR\,cos\varphi+R^2+(b-z)^2}{(a-R)^2+(b-z)^2}}\left\{\left((a+R)^2+(b-z)^2\right)F\left(\frac{\varphi}{2}\middle|-\frac{4aR}{(a-R)^2+(b-z)^2}\right)-\left(a^2-R^2+(b-z)^2\right)E\left(\frac{\varphi}{2}\middle|-\right.\right.}{R((a+R)^2+(b-z)^2)}\right.\right. \tag{9}$$

$$\left.\left.\frac{2a\,sin\varphi\,(a^2+R^2+(b-z)^2)}{a^4+2a^2((b-z)^2-R^2)+((b-z)^2+R^2)^2}\right\}\frac{1}{\sqrt{a^2+R^2-2aR\,cos\varphi+(b-z)^2}}\right]_{\varphi=0}^{\varphi=2\pi} dz$$

where $F(\varphi|m)$ is the incomplete elliptic integral of the first kind, and $E(\varphi|m)$ is the incomplete elliptic integral of the second kind:

$$F(\varphi|m) = \int_0^{\varphi}\frac{d\theta}{\sqrt{1-m\,sin2\theta}}$$

$$E(\varphi|m) = \int_0^{\varphi}\sqrt{1-m\,sin2\theta}\,d\theta$$

In the magnet design of this study, a, b, R, and L were 7, 9.5, 1.25, and 6.2 cm, respectively. M_s is the magnetization of the PM, and $\mu_0 M_s$ is equal to the remnant flux density, B_r. In the magnet system design, a PM with nominal B_r of 1.31 T was employed.

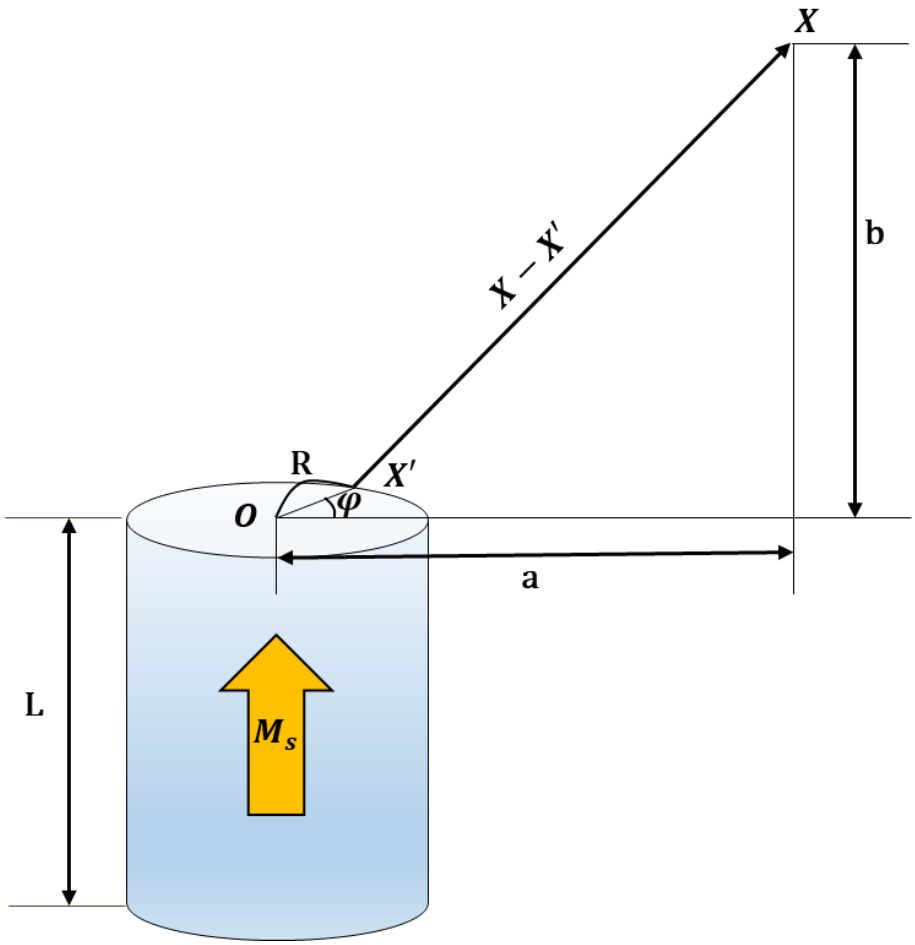

Figure 3 Geometry of an arbitrary cylindrical permanent magnet to calculate its magnetic flux density at an arbitrary point X

3.2.5. Magnetic Field Simulation

COMSOL Multiphysics (version 5.6, COMSOL Inc., Stockholm, Sweden) was employed to guide the design of the magnet system. COMSOL Multiphysics is a commercial FEM software designed to calculate various physical phenomena [29].

For electromagnetic simulation, the physics interface *magnetic field (mf)* available from the *AC/DC module* was adopted to compute the magnetic field. The geometry of the magnet system in FEM simulation was simplified to save the calculation time. The geometry included PMs, magnetic field modulation coils, modulation coil reels, magnetic field sweep coils, and sweep coil reels. Although the sweep and modulation coil geometries could comprise a torus for each turn of the coil wire, the coils were simplified into tubes. Otherwise, the torus geometry would require significant computational time to calculate a large number of meshes composing the tori. The coils were defined using the *multiturn coil* feature. The nonmagnetic components, including the casing and cover, were omitted. The materials applied for each component are listed in Table 1.

Table 1. Material properties used in COMSOL FEM simulation. The electrical conductivity of copper was set as zero. It is followed by the manual of COMSOL Multiphysics. The *multiturn coil* feature is used to prevent the induced current density from flowing through the coil domain in the simulation instead of the wire.

	Relative permeability	Relative permittivity	Electrical conductivity [S/m]	Component
Air	1.0	1.0	0	Ambient space
Copper	1.0	1.0	0	Sweep and modulation coils
MC nylon	1.0	1.0	1.0×10^{-6}	Coil reels, cases
NdFeB	1.05	1.0	5.88×10^{5}	PMs

3.2.6. Magnetic Field Measurement

A magnetic flux density of PMs was measured over a 2-cm diameter of a spherical volume (DSV) at the center of the magnet. According to a dental study, the dimension of the human upper incisor in the oral cavity is 8.73–9.3 mm in width and 10.4–11.2 mm in length [30]. Thus, a 2-cm DSV is wide enough to cover the two upper incisors in a subject's oral cavity. For the conservative assessment, the DSV was larger than the volume occupied by the two upper incisors by a wide margin. The homogeneity was calculated from the following equation:

$$Homogeneity = \frac{B_{max} - B_{min}}{B_{mean}} \times 10^6 \, [ppm] \qquad (10)$$

A gaussmeter (DTM-151 Digital Teslameter, Group 3 Technology, Auckland, New Zealand), in which a hall probe (MPT-141 Hall Probe, Group 3 Technology, Auckland, New Zealand) was attached on a platform moving with a conveyer belt, was used to measure the magnetic field. The magnetic flux density from −7 to 7 cm in the X-axis and −5 cm to 5 cm in the Y-axis at the center of the magnet was measured. In addition to the volume data included in the 2-cm DSV, the magnetic flux density on X-and Y-line profiles was measured for comparison with the FEM results.

The magnetic flux density of a modulation coil was measured using a search coil magnetometer along the X- and Y-axes around the magnet's geometric center. The search coil comprised ten turn copper coils with a radius of 3.82 mm. The region from −3.5 to 3.5 cm along each axis was measured at a 0.5-cm increment. The magnetometer was connected to an oscilloscope so that the peak-to-peak amplitude of the induced voltage was measured. The strength of the modulation field was evaluated by converting the voltage into the magnetic field.

3.2.7. EPR Spectrum Acquisition

An EPR spectrum was acquired to verify the performance of the magnet system combined with an EPR system for *in vivo* tooth dosimetry that had been developed at the Seoul National University. The magnet pole gap was adjusted to 18.4 cm to lower the B_0 closer to the calculated value of 42.9 mT.

The spectrometer system used to acquire the EPR spectra is comprised of the developed magnet system, a spectrometer controller system, a microwave bridge, and a tunable resonator (Figure 4 (a)). The spectrometer systems, except for the developed magnet, were tested using a magnet, which was described in our previous paper [31]. The magnet system' s sweep coils were operated with a bipolar power supply controlled by a controller system. The modulation coils were connected to an amplifier, to which a 21.2-kHz input signal was supplied from the controller system. The acquired data was transmitted to the receiver of the controller.

The circuit connection of the modulation and sweep coils is shown in Figure 4 (b). To operate the modulation coils (L_{M1} and L_{M2} in Figure 4 (b)) at 21.2 kHz, an LC series resonance circuit was used. The sweep coils (L_{S1} and L_{S2} in Figure 4 (b)) were located close to the modulation coil so that AC was induced on it by the AC magnetic field. This induced not only an unintended AC on the sweep coils but also the AC magnetic loss of the modulation field. To reduce this, an LC low-pass filter was connected to the sweep coils.

The EPR spectrum was accumulated ten times for 3 s for each field sweep. Ten spectra were collected for each sample. The peak-to-peak amplitude of the first harmonic signal was estimated. The RIS of two intact human upper incisors were measured after 5- and 30-Gy X-ray irradiation for each. As a reference material, ^{15}N PDT was prepared in a thin Teflon tube after dilution to 0.1 mM.

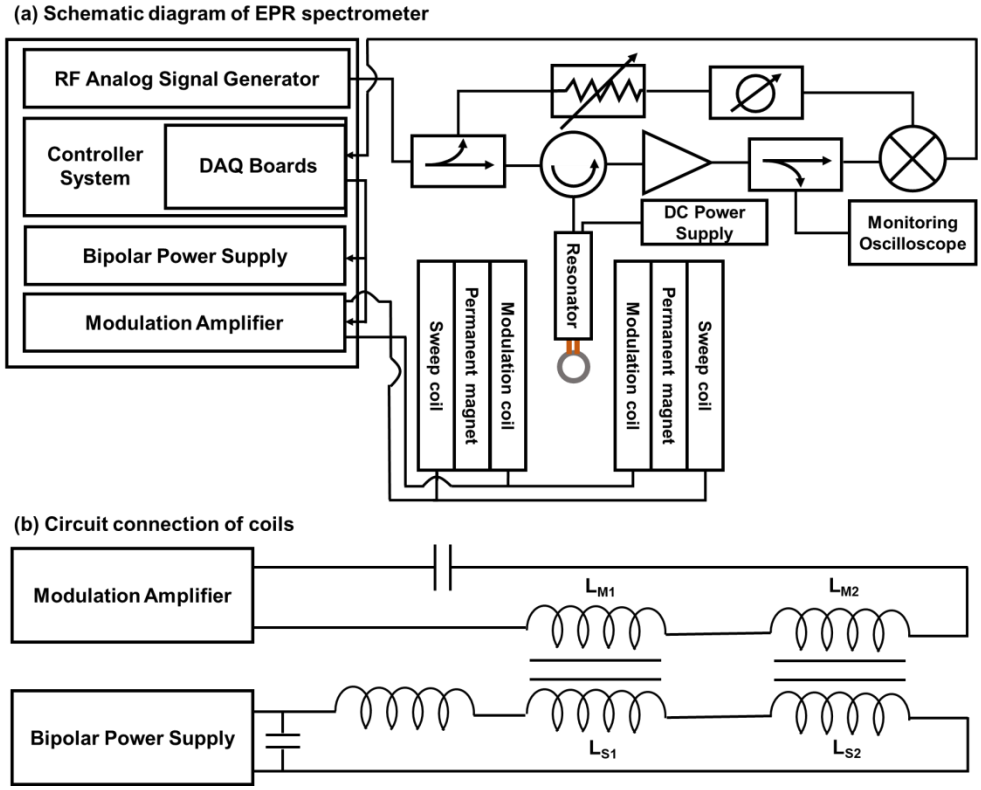

Figure 4 EPR spectrometer connection. (a) Schematic of EPR spectrometer for *in vivo* tooth dosimetry. (b) Circuit connection of modulation coils (L_{M1} and L_{M2}) and sweep coils (L_{S1} and L_{S2}). The LC series resonant is used to operate the modulation coils with 21.2 kHz. In the sweep coil circuitry, the LC low-pass filter is connected to block the AC induced by the AC magnetic field from the modulation coil.

3.3. Results

3.3.1. Characteristics of Prototype Magnet System

In this section, the actual characteristics of the described magnet system are described briefly. The total weight of the magnet was 22 kg. The weight was 27% lighter than that of the *in vivo* tooth dosimetry study by Williams et al. [16]. This was because of the use of higher grade PMs than the benchmarked one. In this study, the N42 grade was used while the N40 or lower were used for the benchmarked one. Another factor that caused the weight decrease was the reduced frame. The frame volume was significantly smaller than the benchmarked Dartmouth magnet.

The pole gap width was 18 cm. The main magnetic field was measured to be 44.5 mT at 2-cm DSV of the magnet system' s center. Its homogeneity was 0.07 mT in the B_0 variation measured along the X-axis in the 2-cm DSV; however, it was estimated to be usable, approximately satisfying the 0.026-mT requirement when a tooth is the subject of measurement. The sweep width was 5.7 mT in the current range of ±9 A, sufficiently requiring the aimed specification. The modulation field amplitude was 0.38 mT.

3.3.2. Magnet System Building

The designed magnet system was manufactured by Hanmi Techwin, Siheung, S. Korea. The developed magnet system is shown in Figure 5. The sweep and modulation coils were independently manufactured and assembled so that they are independently exchangeable in case of a malfunction. The sweep coils are located at the outermost location of the magnet system, whereas the PMs are invisible from the outside (Figure 5 (a)). From the side view of the magnet system, some modulation coils and their wiring are observed (Figure 5 (b)). The modulation coils are wound with reels made of monomer casting nylon, and their outer sides are exposed to air. All the metallic parts, except for the PMs and coils, were made of brass or stainless steel, which are nonmagnetic. The pole gap has a minimum of 17.8 cm and is extendable up to 19 cm by adjusting 16 hexagon nuts, fixing the location of both sides of the magnet system.

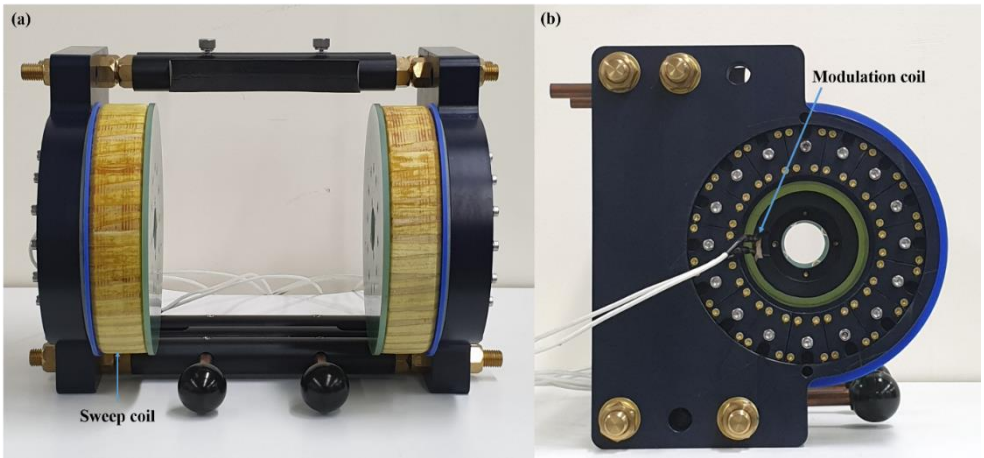

Figure 5 Manufactured magnet system for in vivo EPR tooth dosimetry. PMs are invisible from the outside. (a) Sweep coils are exposed from the front view. (b) Parts of the modulation coils and their wiring are observed in the side view

3.3.3. Prototype Magnet System

The magnetic flux density profiles along the X- and Y-axes are presented in Figure 6 for comparison of the measurement and FEM simulation values. The three profiles in each of Figure 6 (a)-(d) correspond to the PMs only and sweep coils operating ± 4 A. The mean values and homogeneity of the magnetic field density profiles are summarized in Table 2. As described in the Appendix, an analytical calculation was performed to confirm the magnetic flux density of the PMs. The measured homogeneities were higher, especially in Figure 6 (d), owing to the inevitable vibration of the hall sensor during measurements.

After smoothing the profiles with the moving average method, the homogeneity of the Y-axis and XY-plane became 337 and 1600 ppm, respectively.

To determine if the high inhomogeneity was induced by the mechanical vibration, the profile of the magnetic field was remeasured using a Gaussmeter on a stable movable platform. It was manually operated that the measurement was more stable (Figure 7). The results showed similar ones assessed from the original measurements, which high inhomogneity did not originate from the mechanical vibration.

With the smoothed measured data in the Y-axis, the B_0 variation was 0.014 mT, which satisfied the requirement of less than 0.026 mT. However, the raw B_0 variation in the XY-plane was 0.07 mT and not satisfactory for the homogeneity requirement. As mentioned earlier, the actual B_0 variation was smaller than this; the homogeneity was calculated conservatively within a volume larger than the tooth. The B_0 variation of the XY-plane is 0.028 mT if calculated in the region of 1 cm on the X-axis and of 0.2 cm in the Y-axis around the geometric center. This is nearly satisfactory for the 10% linewidth requirement of the RIS. This region could be applied only when one incisor is located at the center.

The magnet system was designed to adjust its pole gap between 18 and 19 cm in case of a situation requiring a change of B_0 strength, which is often caused by a difference (or error) in the remanent flux density of the PM from the nominal value. The variation of the magnetic flux density versus the pole gap distance was calculated in the 2-cm DSV via FEM simulation (Table 3). As the pole gap varied from 18 to 19 cm, B_0 decreased from 43.5 to 41.2 mT. For tuning at the 1.2-GHz system frequency of the entire EPR spectrometer, the pole gap was determined to be 18.4 cm.

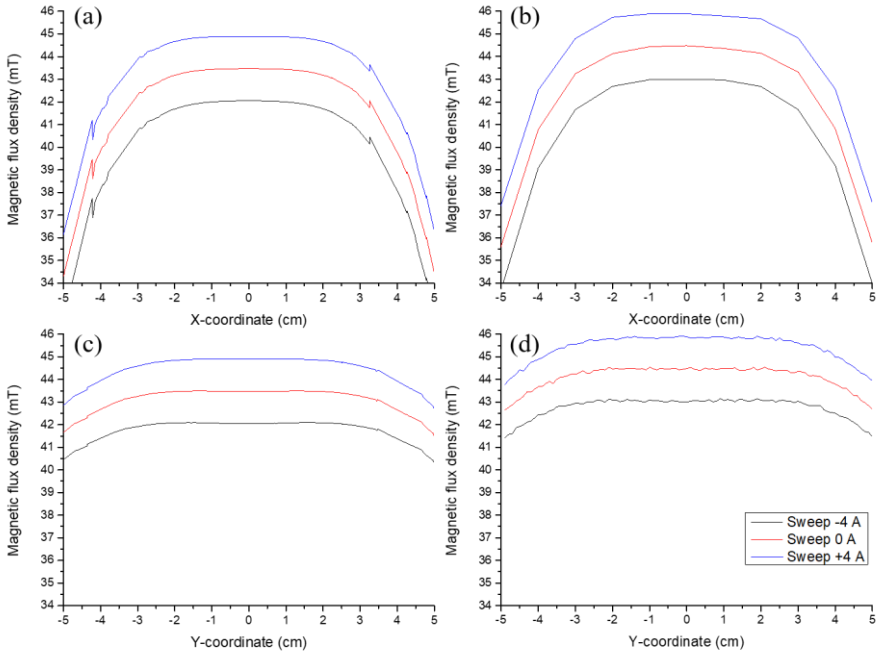

Figure 6 Measured profiles of magnetic flux density along the X- and Y-axes. (a) X-axis profile of FEM results with and without current in sweep coils; (b) X-axis profile of measurement; (c) Y-axis profile of FEM result; (d) Y-axis profile of measurement results. It should be noted that the direction is on the X-axis, and the XY-plane is a horizontal midplane between the pole faces.

Table 2. Mean values and homogeneity of magnetic flux density evaluated for 2−cm DSV. The magnetic flux density evaluated from the measurement is significantly nonuniform. After smoothing the measured profiles, the homogeneity of the Y−axis and XY−plane is 337 and 1600 ppm, respectively. The X−axis is in the direction where the main magnetic field penetrates the two pole faces. The XY−plane is a horizontal midplane between the pole faces.

	X-axis		Y-axis		XY-plane	
	Mean (mT)	Homogeneity (ppm)	Mean (mT)	Homogeneity (ppm)	Mean (mT)	Homogeneity (ppm)
Measurement	44.43	2701	44.47	2923	44.45	4500
FEM	43.46	829	43.47	374	43.46	1258
Analytical calculation	44.06	891	-	-	-	-

Table 3 Magnetic flux density with pole gap extension. The magnetic field and its homogeneity are estimated for 2−cm DSV

Pole gap (cm)	Magnetic flux density (mT)	Homogeneity (ppm)
18.0	43.5	2,183
18.2	43.0	2,162
18.4	42.6	2,129
19.0	41.2	2,577

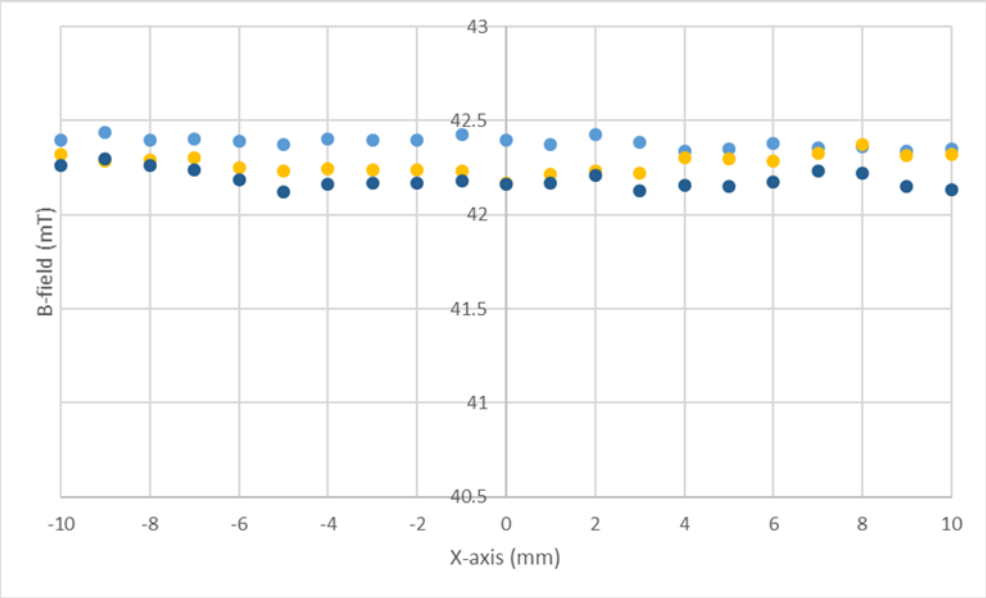

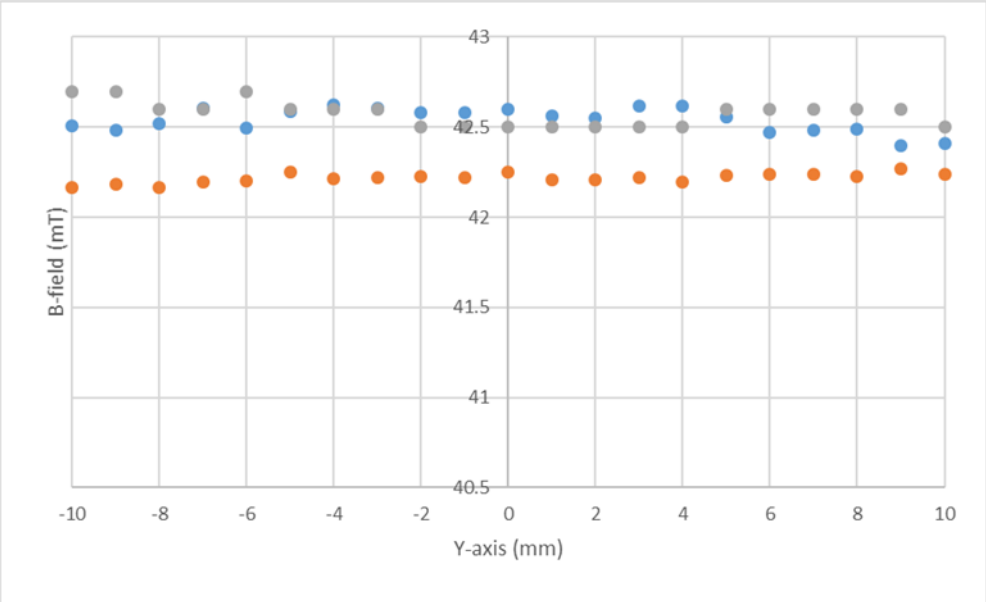

Figure 7 Re-measured magnetic flux density using more stable platform (manually operated axis moving platform). The magnetic flux density was 42.38 and 42.22 mT in the X- and Y-axes, respectively. The homogeneity was 2359 and 2452 ppm, respectively.

3.3.4. Sweep Coil

The magnetic flux density of the sweep coils was measured in the XY−plane. The measurement values were compared with the FEM simulation values (Figure 6). The mean value and homogeneity with a current in the sweep coil are listed in Table 4. After smoothing the measured Y−axis line profile, the homogeneity became 999 and 611 ppm for −4 and 4 A, respectively. The mean value and homogeneity on the XY−plane were evaluated as 45.85 mT and 1381 ppm for 4 A and 43.30 mT and 2350 ppm for −4 A, respectively, after smoothing the measured values. The sweep efficiency was measured as 0.35 mT per Ampere in the range of ±4 A. When a current range of ±9 A was applied at the bipolar power supply, the sweep field ranged from −2.9 to 2.8 mT around B_0, which was sufficiently wide to acquire the EPR spectra of both the tooth RIS and the reference signal of the ^{15}N−PDT.

Table 4. Mean value and homogeneity of magnetic flux density with a current in the sweep coil evaluated for 2−cm DSV. The X−axis is in the direction where the main magnetic field penetrates the two pole faces. The Y−axis is a horizontal plane between the two pole faces.

		X-axis		Y-axis	
Sweep current	Method	Mean (mT)	Homogeneity (ppm)	Mean (mT)	Homogeneity (ppm)
−4 A	Measurement	42.98	698	43.05	3,484
	FEM	42.04	1,288	42.06	583
+4 A	Measurement	45.86	2,181	45.86	2,617
	FEM	44.88	400	44.89	268

3.3.5. Modulation Coil Measurement

The measured magnetic flux density profiles of the field modulation are shown in Figure 8. The peak-to-peak amplitude was 0.38 mT at the geometric center. Additionally, to assess the variation in the magnetic field modulation, the line profiles were measured in the ±1 cm region around the geometric center of the magnet. The homogeneity of the modulation field was 5.7%, 3.6%, and 8.0% along the X-axis, Y-axis, and XY-plane, respectively. Compared with data from another group where the homogeneity of the modulation coil was 5%, these values were less uniform [25]. However, when the region was confined to 1 cm in the X-axis and 0.2 cm in the Y-axis where only an incisor can be located, the homogeneity was 1.8%.

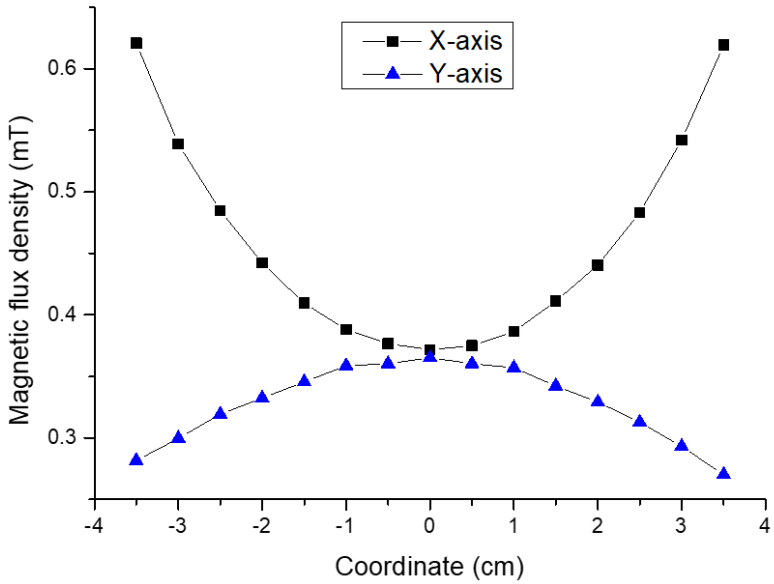

Figure 8 Measured line profile of modulation magnetic field peak-to-peak amplitude along the X- and Y-axis. The X-axis is in the direction of the main magnetic field, whereas the Y-axis is in the horizontal plane between the poles.

3.3.6. EPR Spectrum Acquisition

To fully test the performance of the magnet system integrated with the entire EPR system, it is essential to acquire the EPR spectrum. A tooth was fixed at the geometric center of the developed magnet system. The surface coil of the resonator was contacted to the surface of the tooth (Figure 9 (a)). At each end of the magnetic field sweep, the measured EPR spectrum is shown on the computer's display (Figure 9(b)). Ten sweep data were collected and averaged to produce a spectrum of one tooth.

Figure 10 shows the EPR spectra acquired from the irradiated intact teeth. The spectrum shape was the first derivative of the absorption signal owing to the magnetic field modulation and phase-sensitive detection. In Figure 10, the left peak was the RIS from the tooth, whereas the right one was from the reference material ^{15}N PDT that was simultaneously measured. The signal amplitudes of the reference signal have the same level in both the spectra of the 5- and 30-Gy irradiated teeth. The RIS spectra of the 5- and 30-Gy teeth were distinguishable in amplitude. The peak-to-peak amplitudes of the tooth RIS were 0.16 and 0.83 in arbitrary units for 5 and 30 Gy, respectively.

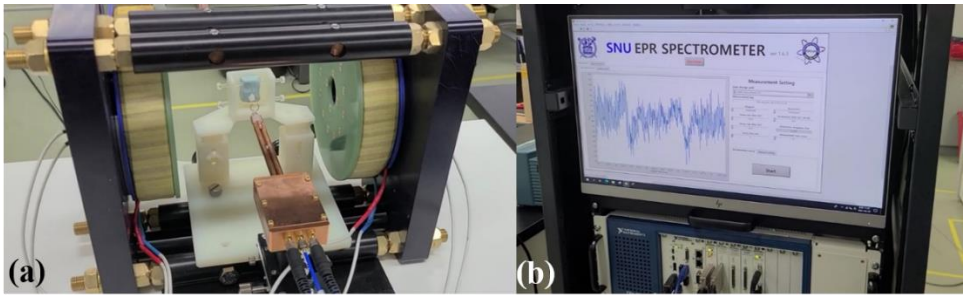

Figure 9 Spectrum acquisition with the developed magnet system: (a) EPR spectra are acquired using a surface coil resonator at the center of the magnet system and (b) measured signals are collected using the controller system and the EPR spectrum is acquired.

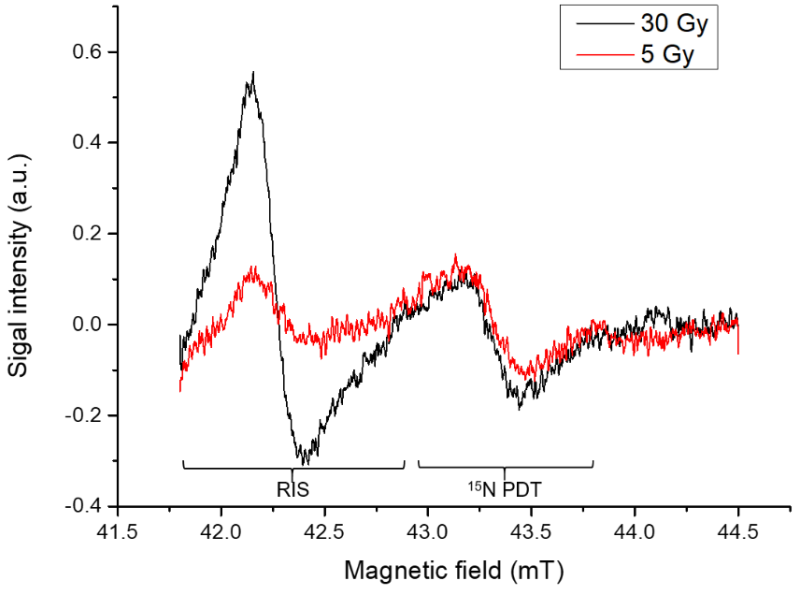

Figure 10 Measured EPR spectrum. Spectrum acquired from 5-(red) and 30-Gy irradiated incisors. Two peaks are shown in each spectrum. The RIS of the tooth (left peak) is distinguishable in amplitude. The reference material, 15N PDT (right peak), has the same height in both spectra.

3.3.7. Thermal Stability of the Magnet

It is known that NdFeB magnets have a temperature coefficient of intrinsic coercivity of approximately −0.10%/°C, which means that the temperature variation of PMs induces the change in the magnetic flux density [32]. The magnetic field shift was observed during long−term EPR measurements (Figure 11). The magnitude of this shift was approximately up to 1.2 mT for the first two hours of operation and then saturated. This may have been due to the temperature rise in the PMs mainly by the modulation coils. This magnetic field shift by the heat should be considered when EPR measurements are performed. To prevent the magnetic field shift during operation, preheating was required when the developed magnet was used. With 2 h of preheating, the magnetic field shift became negligible during further measurements.

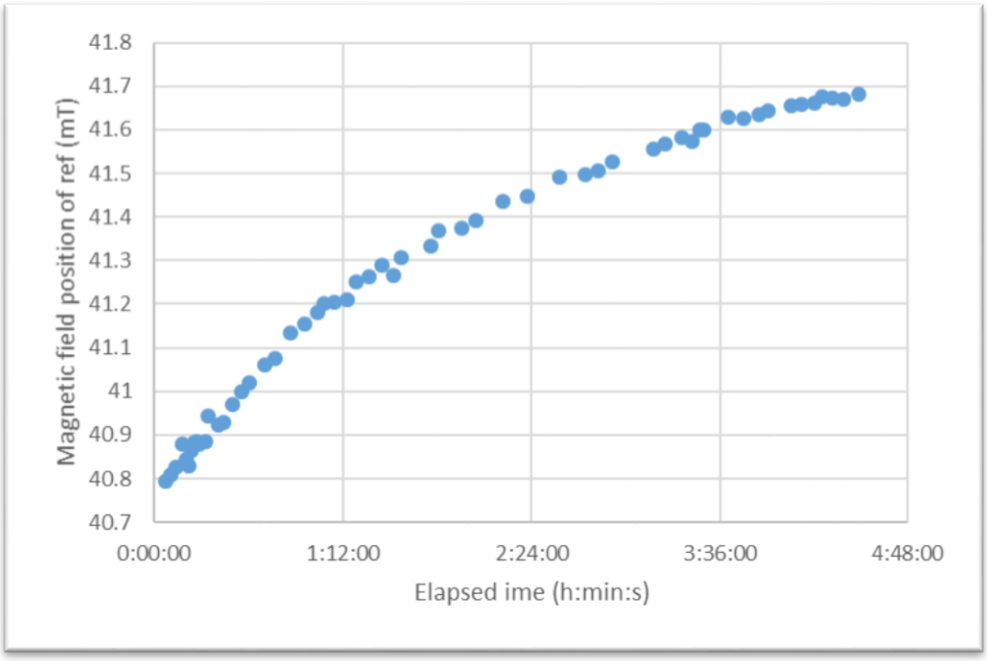

Figure 11 Shifting of EPR spectrum position from the start of the magnet operation with time elapse. The measured EPR spectrum is from ^{15}N−PDT used as the reference sample.

3.4. Discussion

3.4.1. Baseline Distortion of EPR Spectrum

During the first tests to verify the performance of the developed magnet, the distortion of the signal was observed on the EPR spectrum. Figure 12 shows the spectrum acquired when a putty dummy sample was measured with the developed magnet. Although the putty sample itself has no intrinsic characteristic to exhibit a significant EPR signal, a curve−like shape is formed between the two peaks of the reference material signal. Because this magnetic field region is the location where the RIS of the tooth shows its EPR peak, the spectrum in this region is required to be flat without the sample or with the sample with an insignificant EPR level.

It was concluded that the source of this distortion was the magnet itself because it was observed even without the sample in the measurement. A kind of mechanical impact was observed from the magnet once in every end of a sweep.

This impact was found to be the result of the interaction between the PMs and sweep coils. The sweep coils were under the effect of a static magnetic field originating from the PMs. Because of the charges flowing through the sweep coils, they always receive an electromotive force (EMF) by the interaction of the field of the PMs with the charges flowing (current) through the coil wires.

$$\text{EMF: } \vec{F} = \vec{I} \times \vec{B} \tag{11}$$

At every end of the sweep, the direction of the sweep magnetic field is changed say, from +0.3 to −0.3 mT. This abrupt change of the current affects the force applied to the sweep coils with a strong EMF, which creates the movement of the sweep coils. Although the movement of the coil was observed through the impact at the end of the sweep, it was evident that the sweep coils were moved by the EMF during the sweep process. The movement affected the measurement obtained and caused the unexpected

curve-like shape on the EPR spectrum.

The prototype developed magnet was constructed part by part and assembled afterward. Every part had an allowance for the assembling space. The assembly of the sweep coils and their reels had more allowance than the intended design, which allowed the sweep coil to move within a short distance and created an impact when strong EMF was applied.

The distortion was moderated to an insignificant level after the sweep coil structures was re-impregnated in resin epoxy and reassembled. After the re-impregnation, the impact observed at the end of the sweep was significantly moderated. The impregnation process firmly fixed the sweep coils to the reels and the frame of the magnet, keeping the coils from moving even with the EMF.

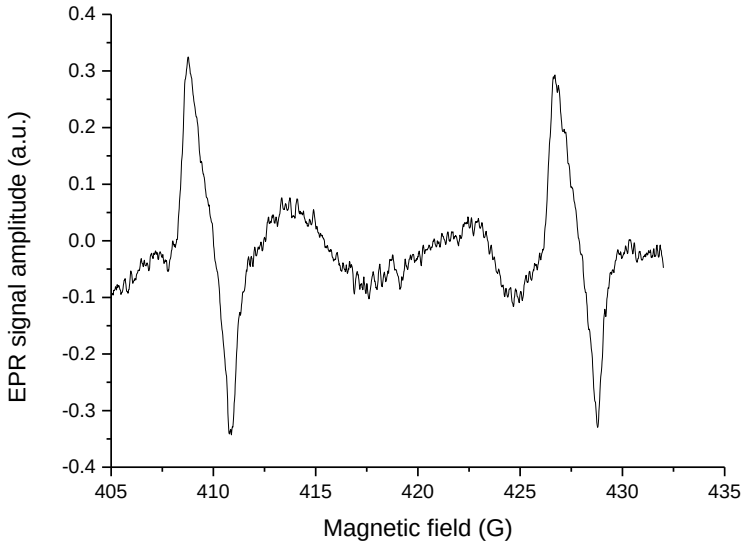

Figure 12 Distortion in EPR spectrum in measurement of a putty dummy with the developed magnet during first trials. A curve-like shape is observed on the magnetic field region between 415 and 425 G although the putty dummy intrinsically has the insignificant EPR signal. The magnetic field region between the two peaks of PDT is the location where the radiation-induced signal of the tooth is formed.

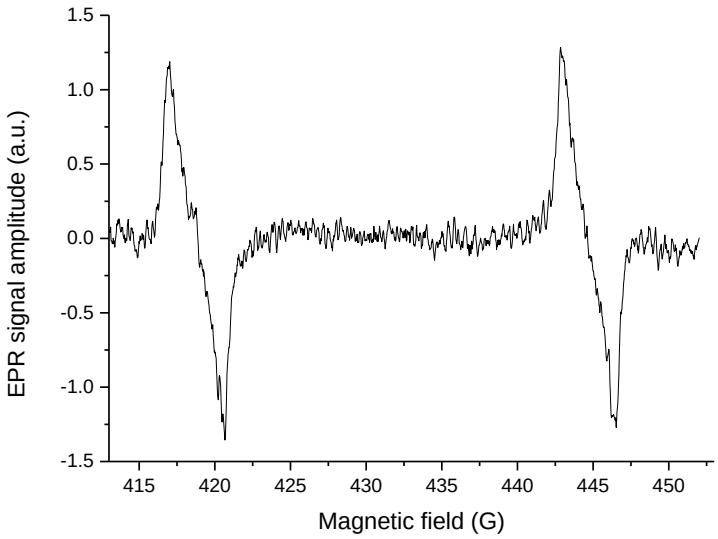

Figure 13 EPR spectrum measured from a putty dummy sample. The spectrum between the two peaks of the reference material became almost flat so that the spectrum of the RIS could be observed without interference.

3.4.2. Calibration of Modulation and Sweep Coils

Before the dosimetry study, the magnet should be calibrated for accurate measurement. For the sweep coils, the relationship between the applied voltage from a bipolar power supply and the varied magnetic field was measured. In the lab setup, the main magnetic field was measured as 44.3 mT. The sweep efficiency was confirmed as 3.8 mT/V. These measured results were parameterized in the measurement program.

For the modulation coils, the modulation field stability was tested by measuring its variance with the time elapse. The modulation coil is the most sensitive part in the magnet system. Because the EPR signal amplitude is directly proportional to the amplitude of the modulation field to a certain point, if the modulation field is unstable, the EPR measurement becomes unstable.

The peak-to-peak modulation field was measured using a magnetometer (Figure 15). To amplify the variance of the field, the magnetometer was attached to one side of the poles where the modulation field was larger than that at the center. The field became weaker with time until the point when approximately 2 h had elapsed. Because the time is taken to damp the oscillation in the LC circuit, the time should be taken before the EPR measurement for stable results.

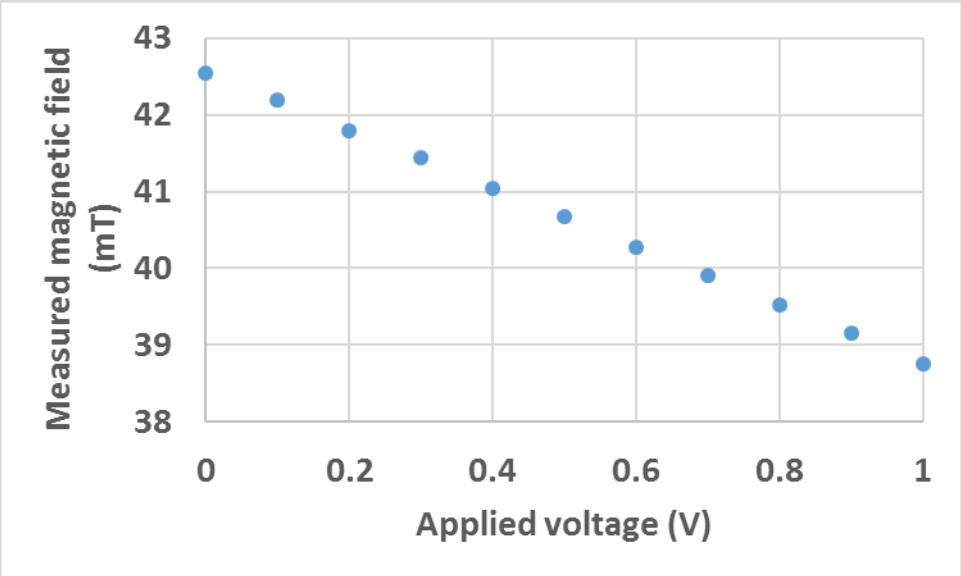

Figure 14 Sweep coil calibrated to the applied voltage from a bipolar power supply.

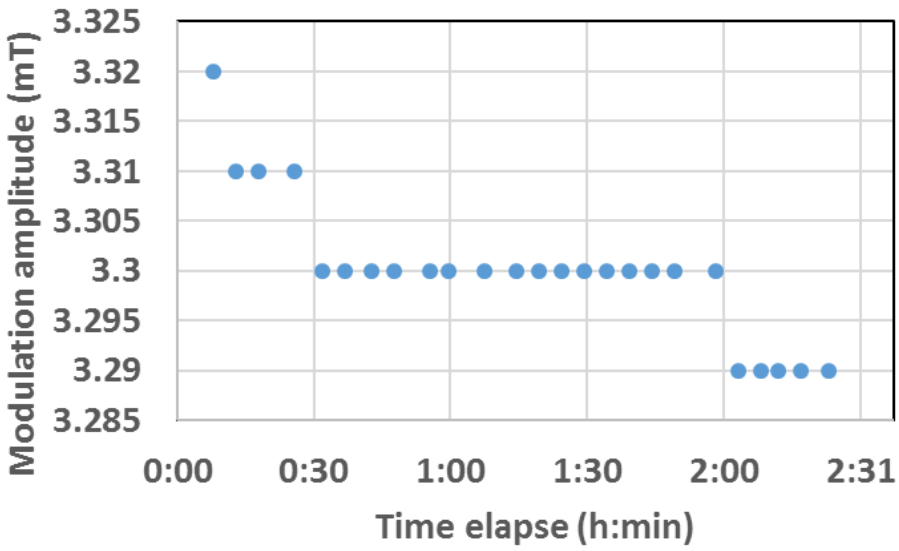

Figure 15 Modulation field measured at one side of the poles. With time elapse, the modulation field become diminished until the elapse point of 2 h. From this point, the field became stable.

3.5. Conclusion of the Magnet Development

A magnet system for *in vivo* EPR tooth dosimetry was designed and fabricated in this study. The fabricated magnet system satisfied the specifications required to perform *in vivo* tooth dosimetry. NdFeB PMs were used to generate the main magnetic field, B_0, which was estimated to be 44.5 mT at the geometric center of the magnet. The field homogeneity was sufficient for application in EPR tooth dosimetry compared to a known RIS linewidth of the tooth spectrum. Furthermore, compared with a 0.26−mT linewidth of the tooth RIS, the modulation field was sufficiently strong to measure the tooth RIS spectra. The range of the sweep coil was 5.7 mT with ±9 A current. It was wide enough to acquire the full EPR spectra of both the RIS and ^{15}N−PDT. The EPR spectra of the irradiated teeth were successfully acquired using the fabricated magnet system. The RIS of the 5− and 30−Gy irradiated teeth were clearly distinguishable.

Chapter 2. In Vivo Dosimetry Method Using Pseudo-In-Vivo Phantom

1. Introduction

Large scale radiation accidents such as the Chernobyl disaster, or the Fukushima Daiichi accident have the potential to involve large populations with exposure to unexpected doses of radiation. Although thousands of victims are potentially exposed to the radiation, providing all the people with treatment for the most severe level of exposure is unlikely. While severely exposed individuals urgently need proper management and treatment, persons that are irradiated but without clinical symptoms require no immediate treatment. Generally, it is known that 2 Gy is the threshold where clinical symptoms occur for an exposed individual. Therefore, it can be inferred that the discrimination of individuals exposed to clinically meaningful doses from thousands of victims is important to effectively concentrate the potential of available treatment. Additionally, especially in the triage of a large scale of victims, screening is required to be fast enough to burden a large throughput within a limited time and with limited manpower.

Although the gold standard for the radiation triage is the chromosome analysis, the assessment takes a long time and skilled workers. This can be a weak point for a triage tool in the assessment of a large number of persons. In this point of fast assessment, in vivo EPR tooth dosimetry has been proposed as a suitable option. It can measure and assess one subject in a few minutes with high throughput. It is relatively easily operated by less skilled operators. Furthermore, in several previous studies, in vivo EPR devices had been developed in light and compact forms so that it could be directly carried with a vehicle to the location of the counter-accident. Moreover, in vivo EPR tooth dosimetry is a unique technique to measure human subjects noninvasively.

For the application of EPR tooth dosimetry to in-vivo

measurements, an EPR dose response calibration curve for in vivo conditions is required. Because the sensitivity of the EPR signal diminishes under in vivo conditions, dose-response calibration data collected in ex vivo conditions cannot be directly applicable to assess the individual exposed dose. By acquiring the EPR dose-response calibration data for in-vivo application, the in vivo EPR tooth dosimetry can be optimized and prepared for application in emergencies [33].

In previous studies on in vivo EPR tooth dosimetry, there have been roughly two methods used to collect data for the in-vivo dose response curve. First, the data are collected by measuring the subjects exposed to the radiation. In this method, the main target subjects are post-treatment patients that have received radiotherapy. Particularly, subjects that have received TBI treatment are regarded as the most suitable subjects [33]. Compared with patients that have received other forms of radiotherapy, TBI subjects have an advantage in that they received relatively uniform doses on their entire body, which is the closest assumable situation to radiation accidents. Another advantage is that the radiation doses that the subjects receive are relatively well trackable by comparison with the prescribed doses. This latter advantage is the main reason for the evaluation of post-treatment patients rather than victims of radiation accidents whose exposed doses are unknown.

Although radiotherapy patients can be evaluated for in vivo data collection, unfortunately, it is difficult to receive consent from the patients owing to their sensitive health condition such as immunity problems. Because patients receive TBI treatment mainly for bone marrow transplant, their deteriorated immunity blocks them from EPR evaluation during the treatment procedure. Here, the second method is applied.

The second method involves the acquisition of EPR data from extracted teeth under conditions mimicking the in vivo condition. Because it is impossible to irradiate a healthy subject for the purpose of collecting EPR dose-response data, alternative methods

were adopted to use extracted human teeth.

Williams et al. used extracted human teeth in an 'in vitro anatomical mouth model', which facilitated the acquisition of the dose-response curve with effects of anatomical variations, and microwave properties of the oral cavity [5]. Kobayashi et al. evaluated in vivo tooth dosimetry with the 'complex mouth model' more thoroughly [34]. It reflected the microwave properties in the oral cavity by controlling the Q factor of the resonator. They collected the dose-response EPR data of the teeth using the complex mouth model. For comparison, other dose-response calibration data were collected from the same teeth under in vivo conditions. The teeth were fixed as dentures, which were equipped on a subject with a missing tooth gap. This study provided significant evidence that the EPR data collected from the extracted teeth can fully be an alternative of in vivo measurements by controlling the Q factor.

In the measurement of the EPR spectrum, the relative sensitivity of the signal is determined by the following characteristics of the resonator; the amplitude of the magnetic field efficiency induced by the applied power at the resonator, the filling factor, and the Q factor [35]. Among these factors characterizing the relative sensitivity, it can be inferred that the magnetic field efficiency from the resonator is the same under any circumstances if the same devices are used. The filling factor is related to the relative locations and shapes of the resonator coil and the subject tooth [36]. Therefore, the filling factor varied based on the subject teeth's relative location and geometry. This variation was proved to be moderated by applying correction using the enamel area, or volume of the teeth [31]. The Q factor is the most significant factor among these three factors. For the quantitative comparison of the EPR signal with the reproducibility, the Q factor should be measured or kept constant [37].

Although the aforementioned study by Kobayashi et al. presented a great alternative method to detour direct in-vivo measurement to acquire the dose-response data, in the actual case

of in vivo measurements, a variance in the Q factor between individuals could be observed. The difference in the Q factor incurs a difference in the sensitivity of the EPR signals, which makes it difficult to adopt the prepared dose-response calibration curve for the dose assessment.

In this study, a method for further Q factor control is proposed to apply the dose-response curve to an in-vivo situation with an arbitrary Q factor. If the EPR dose-response calibration curve is flexibly controllable following the varied Q factor of the in-vivo subjects, dose assessment can be adaptively performed for all the possible Q factors of subjects. EPR tooth dosimetry was performed using extracted teeth with the Q factor controllable 'pseudo-in-vivo phantom'. To verify the performance of the proposed method, post-radiotherapy patients were evaluated for in vivo tooth measurements.

2. Materials and Methods

2.1. Pseudo-In-Vivo Phantom

The pseudo in vivo phantom was fabricated with the tissue equivalent material based on the formula proposed by Robinson et al. [38]. Gelatin (Gelatin from porcine skin, Type A, Sigma-Aldrich, Burlington, United States), ethylene glycol, sodium chloride, and highly purified water (Daejung Chemicals & Metals, Siheung, Republic of Korea) were mixed in a ratio of 2:48:40:10 to form a pseudo in vivo phantom. The mixture was heated and poured into a mold to form a cuboid shape with a rectangular hole (Figure 1). This phantom shape was created to insert a tooth fixed in the dental impression material, putty (Exafine Putty Type, GC Corporation, Tokyo, Japan) phantom and move it backward and forward in the rectangular hole. By deepening the depth of the tooth phantom, the influence of the pseudo-in-vivo phantom became stronger resulting in a decrease in the Q factor. The pseudo in vivo phantom was thoroughly covered with plastic wrap to prevent the evaporation of water content.

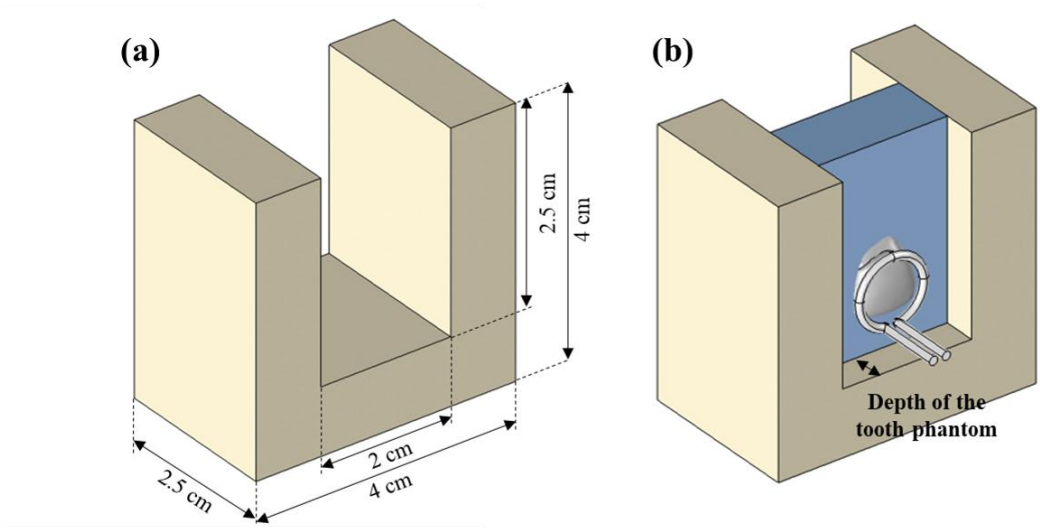

Figure 16 Geometry of pseudo-in-vivo phantom (a) and description of the depth of the tooth (b)

2.2. Q Factor Measurements

The Q factor was measured to verify its change under the presence of the pseudo in vivo phantom. The measurement was performed with the coil of an EPR resonator contacted on the surface of the tooth while the resonator was connected to the network analyzer. The scattering parameter S_{11} was recorded with a 200 MHz span. From the recorded S_{11}, the Q factor was calculated using following equation;

$$Q\ \ factor = \frac{f_{res}}{Bandwidth} \tag{12}$$

where f_{res} is a resonance frequency, in which the S11 shows the minimum value. The bandwidth was calculated by subtracting the frequencies of two points where the S11 is 3 dB lower than the baseline value.

The Q factors were acquired from four extracted human maxillary central incisors with and without the pseudo in vivo phantom. With the presence of the pseudo in vivo phantom, the Q factor was measured by changing the position of the tooth phantom in the pseudo in vivo phantom. The position was defined as the depth of the tooth in the pseudo-in-vivo phantom. The depth was measured as the length between the surface of the pseudo-in-vivo phantom and the surface of the putty part of the tooth phantom (Figure 16). The teeth were evaluated at depths from −2 to 5 mm with a 1 mm interval.

Additionally, the Q factor was assessed under in vivo circumstances to confirm that the variation of the Q factor by the pseudo in vivo phantom covered the range that appeared under the real in vivo conditions. To evaluate the distribution of the in vivo Q factors, six volunteers were measured using the same setup as that of the extracted teeth.

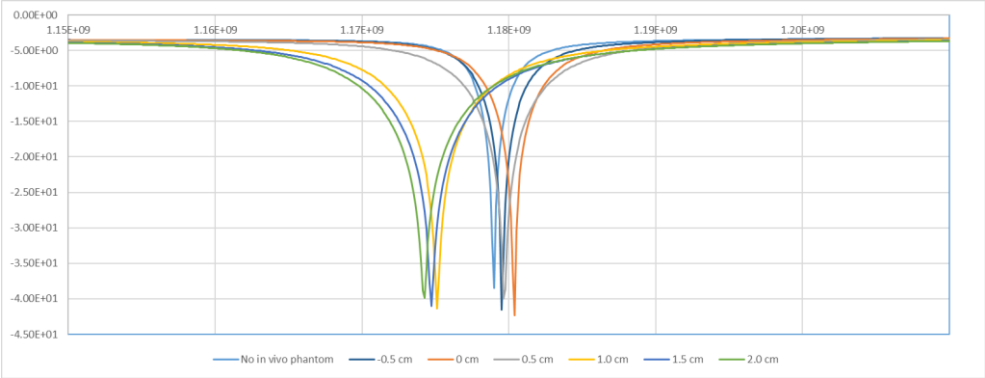

Figure 17 S_{11} scattering parameters measured from the tooth with and without the pseudo-in-vivo phantom. The Q factors were calculated from these.

2.3. Tooth Irradiation

A total of four human maxillary incisors were prepared to evaluate the effect of the pseudo *in vivo* phantom. Each tooth was fixed in the dental putty, which was cut into the same size to the area of the rectangular hole in the pseudo-in-vivo phantom. The size was 2×2.5×1 cm^3. As mentioned, the relative position of the tooth in the pseudo-in-vivo phantom was determined by the position of the surface of the putty part. Therefore, it was important to maintain the protruding height of the tooth when fixing teeth in the dental putty. The teeth fixed in the dental putty were irradiated to 0, 1, 2, 5, and 10 Gy with 220 kVp X-ray using the XRad-320 Irradiator (Precision X-Ray Inc., Madison, CT, United States).

Further X-ray doses were transferred to the same teeth to verify the signal sensitivity of the 6 MV photon beam. Because the dose-response calibration data were collected using a 220 kVp X-ray beam when post-radiotherapy patients had been treated with a 6 MV photon beam from a clinical linear accelerator (Elekta Versa HD, Elekta, Stockholm, Sweden), the difference in the EPR signal sensitivity between the two beams should be confirmed and reflected. Therefore, a total 10 Gy was transferred with the surface of the teeth at the d_{max} in the phantom. The irradiation geometry for both beams is shown in Figure 19.

Both irradiators were calibrated to the absorbed dose to water. The XRad-320 Irradiator was calibrated on the absorbed dose to water at the surface following the AAPM TG-61's in-air method. The clinical linear accelerator was calibrated following the AAPM TG-51 protocol, which was based on the absorbed dose to water.

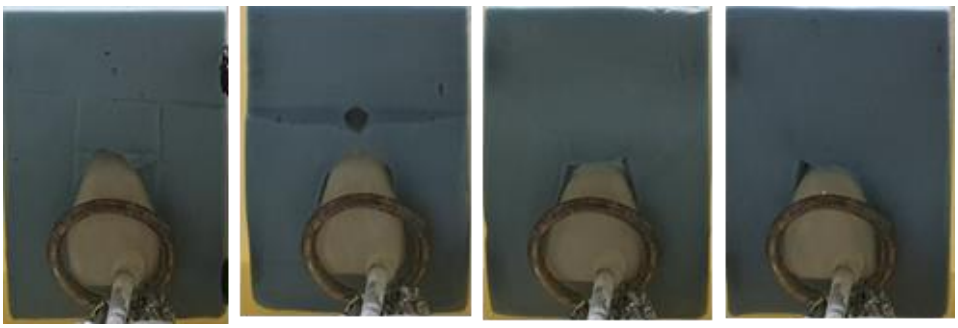

Figure 18 Teeth used for the dose−response data collection.

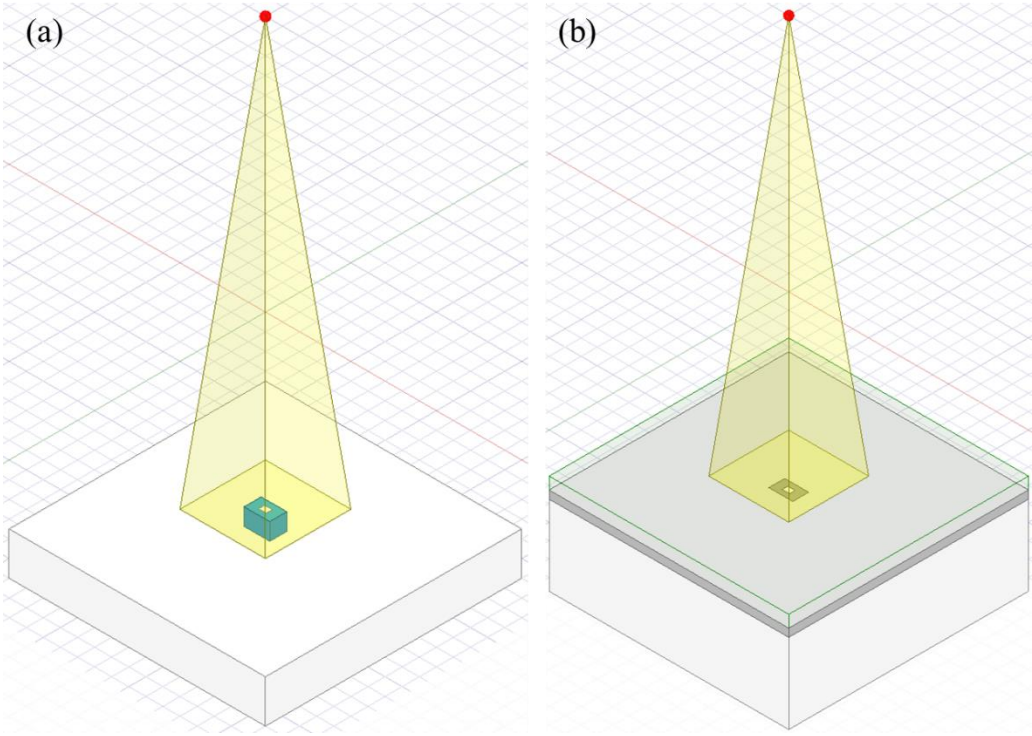

Figure 19 Irradiation geometry for 220 kVp (a) and 6 MV (b). The irradiator for the 220 kVp beam was calibrated for absorbed doses at the water surface, and the 6 MV beam for absorbed doses in water

2.4. EPR Instrument and Measurement

A CW EPR spectrometer developed in a previous study was used for the EPR measurements [31]. Only the magnet system was replaced by the newly developed one for in the vivo tooth dosimetry study [39]. The performance of the developed magnet and combined system were also verified in the previous study.

The EPR dose-response data were collected to plot the calibration curves from the teeth with and without the pseudo-in-vivo phantom. The results of the measurements can be affected by the positioning difference of the tooth in both situations. To avoid affecting the results, the relative position of the tooth to the resonator coil was carefully adjusted to be the same (Figure 20). To match the vertical position of the tooth to that with the pseudo-in-vivo phantom, a support was added under the tooth when the phantom was not used. When the pseudo-in-vivo phantom was used, the EPR spectra were measured at depths of −2, 0, and +2 mm. At a data point of the teeth at each depth, a total of 20 spectra were collected. For each spectrum, a median value of 10 sweeps of 3 s was used. The RIS in each spectrum was used to assess the EPR response. The mean value of the twenty peak-to-peak values of the RIS spectrum were used as the signal amplitude for each data point of the dose-response calibration curve.

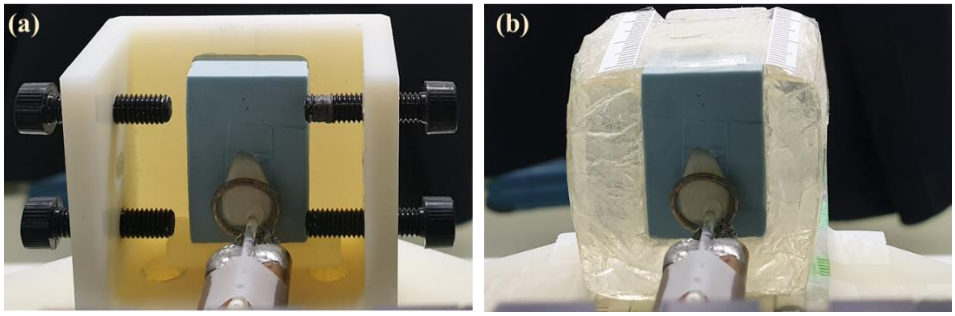

Figure 20 Relative position of the tooth to the resonator coil. (a) The vertical position of the tooth was adjusted by a paraffin wax support when the pseudo in vivo phantom was not in use. (b) When the pseudo in vivo phantom was in use, a ruler was attached beneath the pseudo in vivo phantom to double-check the depth of the tooth in the measurement.

2.5. Correction with Area of Tooth Enamel

The acquired dose-response calibration curves were corrected with the area of the tooth enamel. As aforementioned, the filling factor is one of the main factors affecting the sensitivity of the EPR signal. It is affected by the teeth' s relative location and geometry to the resonator coil. Although the use of volume is a superior way to correct the geometric effect of a tooth more effectively, the volume of the tooth enamel cannot be measured from a tooth in a subject' s oral cavity [31].

Correction with the enamel area is also proved to be useful for enhancing the dose-response curve from teeth of varied sizes [31]. Additionally, this area correction is applicable to in-vivo measurements by taking a picture of the subject' s tooth. The enamel area was measured based on the longest height and width of the tooth enamel [31, 40].

Using the equation proposed by Park et al. the relative sensitivity of the dose-response was calculated from the area of the tooth enamel [31].

$$(\text{Relative sensitivity}) = 0.187 \times (\text{area of tooth enamel}) - 0.642 \qquad (13)$$

$$k_{geo} = \frac{(Mean\ value\ of\ the\ relative\ sensitivities\ from\ samples)}{(Relative\ sensitivity\ of\ a\ sample)} \qquad (14)$$

The calculation of the corrected geometric effect is applied using the following equation;

$$\text{sensitivity} = \text{k}_{geo} \times sensitivity_{tooth} \qquad (15)$$

where, k_{geo} is a correction factor for the sensitivity of the dose-response curve by the tooth enamel area.

2.6. Post-Radiotherapy Patients In Vivo Dose Assessment

Post-treatment patients were evaluated to verify the Q factor control method. The patients had received TBI treatment and were completely cured at St. Vincent's Hospital in Korea. Two subjects participated in the verification. The participants are listed in Table 5. From the subjects, EPR spectra were collected for 1 h. During the EPR measurements, the subjects were asked to hold their breath for 10 s for the spectrum acquisition. For each breath holding, data of two sweeps were acquired with 3 s per sweep. After completing the measurements, fully available spectra were collected and assessed. Additionally, the S_{11} scattering parameter was recorded to measure the Q factor calculation. A photograph of the subject' s teeth was taken for the geometric-correction using the enamel area.

Table 5 Participants in the dose assessment. All subjects had received TBI treatment.

Subject ID	Age	Biological gender	Prescription
Patient 1	55	Female	4 Gy / 4 Fractions / Bilateral
Patient 2	27	Female	12 Gy / 8 Fractions / Bilateral

3. Results and Discussions

3.1. Measurement of Quality Factor

In vivo Q factors measured from six volunteers are shown in Figure 21; they range from 60 to 101. The variance of the in vivo Q factor is mainly originated from the proximity of the resonator coil to the tissue. The size of the subjects' teeth varies between individuals. In the case of S3 whose tooth size was smaller than other volunteers, it was inevitable for the resonator coil to be located closer to the gum during the Q factor measurement. This is the main evidence for the necessity of the controlling Q factor.

The Q factor control performance of the pseudo-in-vivo phantom was measured from four extracted teeth (Figure 5). By varying the depth in the phantom, the Q factor could be controlled in the range from 68 to 111. The depth of -2 mm indicates that the surface of the putty fixed with the tooth is protruded from the phantom by -2 mm. From the comparison of the Q factor measured from the volunteers, the pseudo-in-vivo phantom can simulate the in vivo Q factor with high coverage.

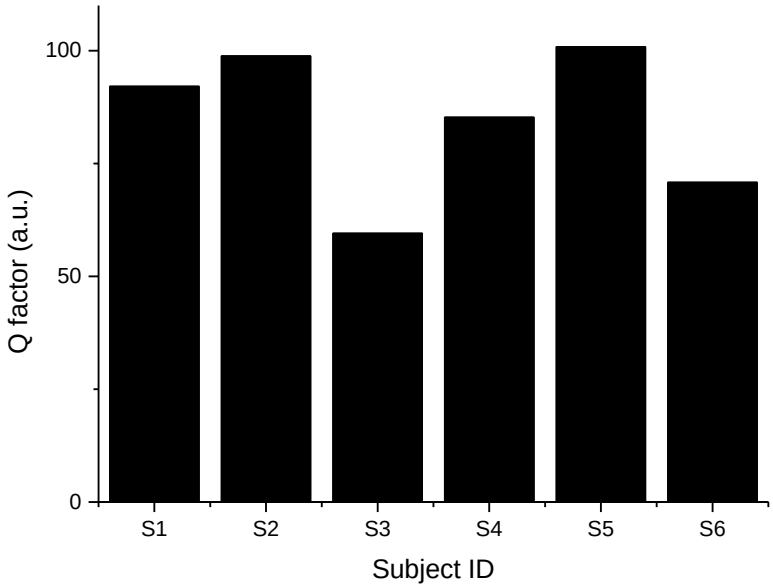

Figure 21 Q factor measured from volunteers without irradiation. There was a variance between subjects.

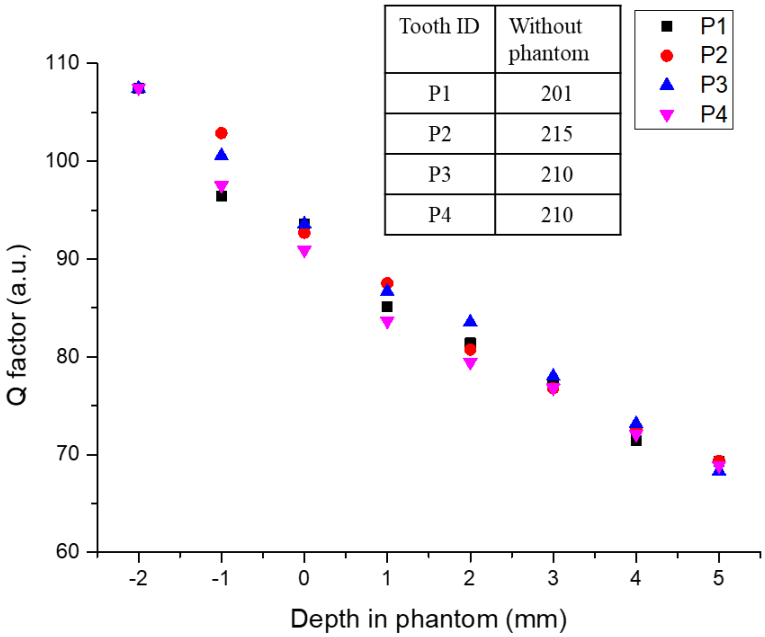

Figure 22 Q factor measured from four maxillary central incisors varying the depth in the pseudo-in-vivo phantom. The teeth were used to collect data for the dose-response curves. The measured Q factors were used to evaluate the relationship of Q factors to the sensitivity, and background signal.

3.2. Dose-Response Calibration Curve

Dose−response calibration curves were acquired from the measurements (Figure 23). Before constructing the calibration curves, the measured RIS was corrected with the area of the tooth enamel using equation (2). The measured area of the teeth enamel and the applied correction factors, k_{geo}, are listed in Table 6.

It was confirmed from the dose−response calibration curves that the sensitivity of the calibration curve decreased with the phantom depth as expected. This verified the function of the pseudo−in−vivo phantom in the control of the Q factor. Additionally, the intercepts of the curves, which are the background signals decreased with the phantom depth.

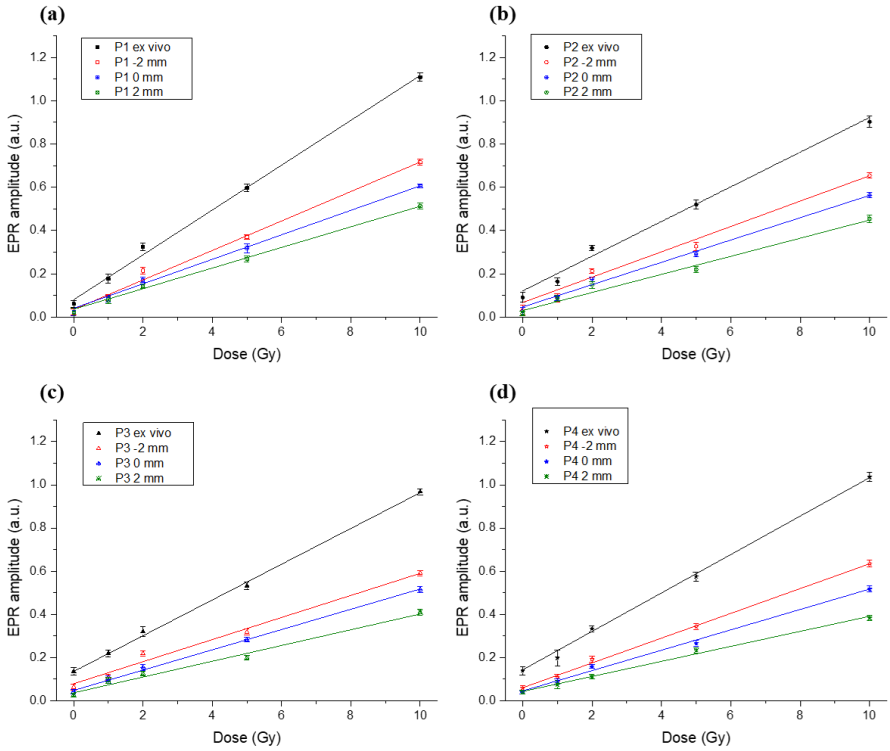

Figure 23 Calibration curves with and without pseudo-in-vivo phantom from four extracted human teeth. Graphs in (a)-(d) show calibration curves from each tooth, P1 - P4, respectively. The EPR amplitudes are re-calculated values after the geometric correction using the enamel area. As the depth of the tooth in the pseudo-in-vivo phantom increases the sensitivity (slope) of the calibration curve decreases owing to the decrease in the Q factor. Lower background signals (intercept of the calibration curve) are also observed at a deeper phantom depth.

Table 6 Enamel area measured from four incisor teeth used to collect data for dose-response calibration curves. The geometric correction factor, $\boldsymbol{k_{geo}}$ was calculated using equation (3).

	P1	P2	P3	P4
Height of tooth enamel (mm)	11.7	11.0	10.9	10.7
Width of tooth enamel (mm)	8.9	8.7	9.7	9.1
Enamel Area (mm^2)	103.2	96.0	105.3	96.63
Relative sensitivity (Gy^{-1})	0.113	0.104	0.115	0.105
Mean relative sensitivity (Gy^{-1})	0.109			
k_{geo}	0.970	1.047	0.949	1.040

3.3. Sensitivity and Background Signal of an Arbitrary Q Factor

As confirmed from the calibration curves, the Q factor affects the sensitivity, and the background signal of the EPR signal. The relationship of the Q factor with the sensitivity, and the background from the measurements are shown in Figure 24. A linear regression line was plotted for each relationship. From this linear regression line, the sensitivity and background signal could be calculated for an arbitrary Q factor. With this new sensitivity and background signal, a new dose-response calibration curve was calculated for a Q factor measured from a post-treatment patient. The parameters for the calculation are listed in Table 7.

In the relationships of the Q factor to the dosimetric sensitivity and the background signal, there are variations in the Q factor from the regression curve (Figure 24). The confidence interval (CI) should be considered when calculating the sensitivity and background signal using the Q factor. The dose-response curve may be different from the nominal value calculated from the regression curve owing to this error as shown in Figure 25. This error leads to the dose estimation listed in Table 8.

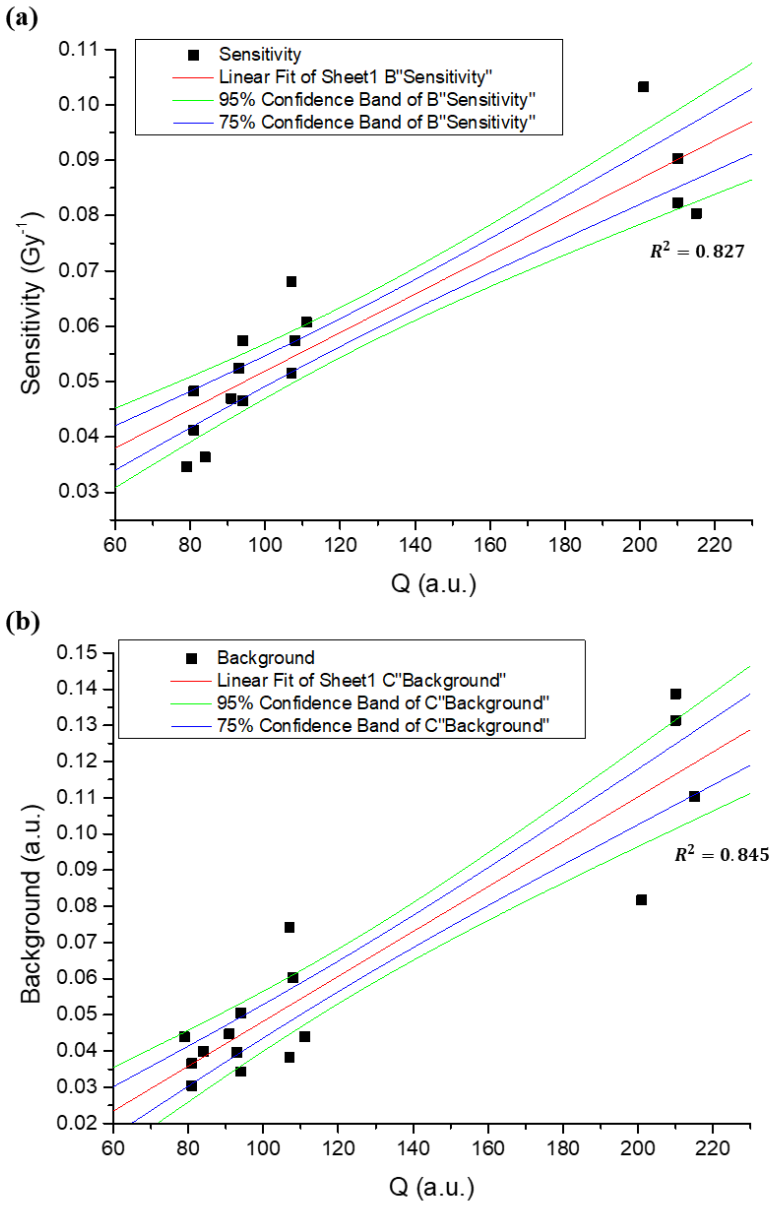

Figure 24 Relationships of the Q factor with dosimetric sensitivity (a), and background signal (b). Both relationships exhibit linear regressions.

Table 7 Parameters calculated from relationships of the Q factor with the dosimetric sensitivity and background signal. From these parameters, the sensitivity and background signal for an arbitrary Q factor are calculated

	Slope	Intercept
Sensitivity	3.474×10^{-4}	1.721×10^{-2}
Background signal	6.180×10^{-4}	-1.357×10^{-2}

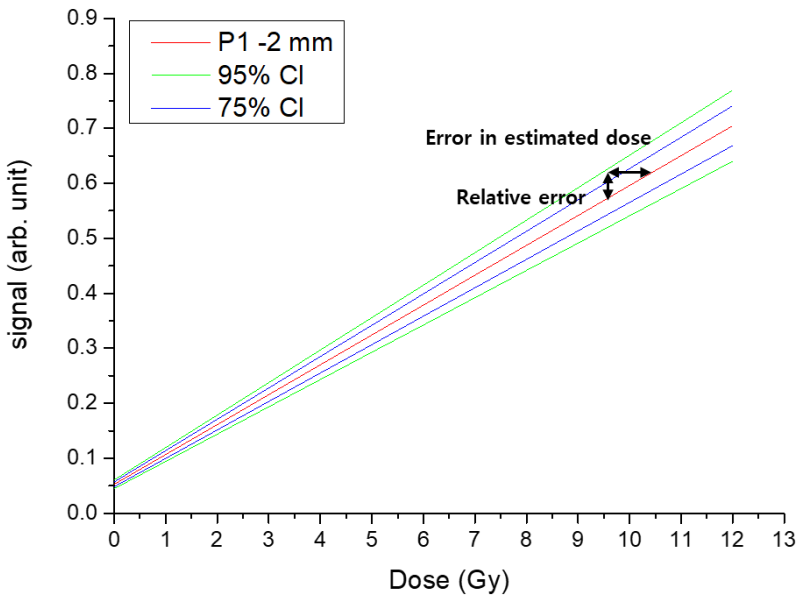

Figure 25 Considered error in dose−response curve induced by the confidence interval in Q factor distribution

Table 8 Confidence interval (CI) in estimating the irradiated dose for each Q factor in the Q factor distribution shown in Figure 24

	Q factor											
	95% CI						75% CI					
Dose (Gy)	60	70	80	90	100	110	60	70	80	90	100	110
0	0.32	0.26	0.22	0.19	0.16	0.14	0.18	0.15	0.12	0.10	0.09	0.08
1	0.51	0.42	0.35	0.30	0.25	0.22	0.28	0.24	0.20	0.17	0.14	0.13
2	0.69	0.58	0.48	0.41	0.35	0.31	0.39	0.32	0.27	0.23	0.20	0.17
3	0.88	0.73	0.61	0.52	0.45	0.39	0.49	0.41	0.34	0.29	0.25	0.22
4	1.07	0.89	0.75	0.63	0.54	0.48	0.60	0.50	0.42	0.35	0.30	0.27
5	1.26	1.05	0.88	0.74	0.64	0.56	0.71	0.59	0.49	0.41	0.36	0.31
6	1.45	1.20	1.01	0.85	0.73	0.64	0.81	0.68	0.56	0.48	0.41	0.36
7	1.64	1.36	1.14	0.96	0.83	0.73	0.92	0.76	0.64	0.54	0.46	0.41
8	1.83	1.52	1.27	1.07	0.92	0.81	1.02	0.85	0.71	0.60	0.52	0.46
9	2.01	1.68	1.40	1.18	1.02	0.90	1.13	0.94	0.78	0.66	0.57	0.50
10	2.20	1.83	1.53	1.29	1.11	0.98	1.23	1.03	0.86	0.73	0.62	0.55

3.4. Verification of Sensitivity Difference Between Two Irradiation Situations

3.4.1. Experimental Verification

Because the doses measured from the post-radiotherapy patients were irradiated by a 6 MV X-ray beam while the dose-response calibration curve was acquired from 220 kVp X-ray beam, the EPR data should be corrected for the difference in the energies.

An additional 10 Gy of the water-absorbed dose was transferred to the teeth used to acquire the dose-response curves with the 6 MV photon beam used for the patient treatment.

The increased EPR signal amplitudes of the teeth by the further 6 MV irradiation were plotted on the pre-acquired calibration curves (Figure 26). Each increased signal intensity was assessed for each tooth (Table 9). The water-absorbed doses were assessed as 1.98, 1.78, 2.68, and 2.00 Gy from teeth P1, P2, P3, and P4, respectively. The mean dose was 2.11 Gy showing the 4.74 times difference;

$$\frac{Sensitivity_{220\ kVp,\ enamel}}{Sensitivity_{6\ MV,\ enamel}} = 4.74 \qquad (16)$$

This discrepancy occurs mainly because of the difference in the mass energy absorption coefficient of the tooth enamel from that of the water between the two energies.

For a clear view and understanding, the increased signal by the additional 6 MV irradiation of the experimental situation was visualized in Figure 27. The dose-response curve was reconstructed using the sensitivity, whereas the background signal was calculated with Q factor 209, which was the average Q factor of the four teeth P1-P4;

① When the 10 Gy water-absorbed dose was irradiated with the 220 kVp beam on the tooth, the EPR signal was increased by 1.01386. At this point, the dose-response curve was acquired.

② Further, the 10 Gy water-absorbed dose was irradiated with

the 6 MV beam. The increased signal intensity by the additional irradiation was 0.1894, which was equivalent to 2.11 Gy on the dose-response curve of the 220 kVp beam.

③ Because the dose delivered to the tooth was the same as the 10 Gy water-absorbed dose in both the 220 kVp and 6 MV photon beam, this could be expressed as;

$$\mathbf{220\ kVp}: \frac{\mathbf{1.01386 - 0.1158}}{\mathbf{10\ [Gy]}} = \mathbf{0.08981\ [Gy^{-1}]} \tag{17}$$

$$\mathbf{6\ MV}: \frac{\mathbf{1.20325 - 1.01386}}{\mathbf{10\ [Gy]}} = \mathbf{0.01894\ [Gy^{-1}]} \tag{18}$$

$$\frac{\boldsymbol{sens_{220kVp}}}{\boldsymbol{sens_{6MV}}} = \frac{\mathbf{0.08981\ [Gy^{-1}]}}{\mathbf{0.01894\ [Gy^{-1}]}} = \mathbf{4.743} \tag{19}$$

where $\boldsymbol{sens_E}$ is the sensitivity for each energy E.

Because the same amount of the water-absorbed dose to the tooth increased by a different amount of the signal intensity, it would be appropriate for the sensitivity of the two energies to be different. Because the difference between both energies is the sensitivity of the dose-response, the dose-response curve of each energy is expressed separately (Figure 28). From the viewpoint of the sensitivity, the dose-response curves can be expressed as;

$$\frac{\boldsymbol{signal_{220kVp}} - \boldsymbol{BKS(Q)}}{\boldsymbol{sens_{220kVp}(Q)}} = \boldsymbol{D_{water}} \tag{20}$$

$$\frac{\boldsymbol{signal_{6MV}} - \boldsymbol{BKS(Q)}}{\boldsymbol{sens_{6MV}(Q)}} = \boldsymbol{D_{water}} \tag{21}$$

where $\boldsymbol{signal_E}$ is the measured signal when irradiated by the photon with the energy E, $\boldsymbol{BKS(Q)}$ is the background signal measured without the irradiation of the sample with the Q factor, Q, and $\boldsymbol{sens_E(Q)}$ is the sensitivity of the dose-response curve for the photon energy E normalized by the area effect of a specific tooth

($\boldsymbol{k_{geo}}$) at the Q factor, $\boldsymbol{Q}$. The sensitivity is calculated by the equation proposed by Park et al. [31].

$$\boldsymbol{sens_E = sens_{spec,E} \times k_{geo}} \tag{22}$$

In the equation of the dose-response curve, the numerator, $\boldsymbol{signal_E - BKS}$ is the net increase of the signal by the irradiated dose, $\boldsymbol{D_{water}}$;

$$\frac{\boldsymbol{signal_E - BKS}}{\boldsymbol{sens_E}} = \frac{\boldsymbol{(net\ increase\ of\ signal)}}{\boldsymbol{sens_E}} = \boldsymbol{D_{water}} \tag{23}$$

Moreover, the net increase of the signal is induced by the radiation dose that the tooth absorbed;

$$\boldsymbol{(net\ increase\ of\ signal) \propto D_{E,enamel}} \tag{24}$$

Based on the energy dependence study of the EPR tooth dosimetry by Ivannikov et al., there is no significant signal difference when the absorbed dose in tooth enamel is the same over 37 keV [41]. Therefore, between the 220 kVp and 6 MV beams, the following relationship stands;

$$\left[\frac{\boldsymbol{(net\ increase\ of\ signal)}}{D_{220kVp,enamel}}\right]_{220kVp} \cong \left[\frac{\boldsymbol{(net\ increase\ of\ signal)}}{D_{6MV,enamel}}\right]_{6MV} \tag{25}$$

From the equation for the dose-response curve, this relationship can be rewritten as follows;

$$\frac{D_{220kVp,enamel}}{D_{6MV,enamel}} \cong \frac{\boldsymbol{(net\ increase\ of\ signal)_{220kVp}}}{\boldsymbol{(net\ increase\ of\ signal)_{6MV}}} = \frac{\boldsymbol{sens_{220kVp} \times D_{water}}}{\boldsymbol{sens_{6MV} \times D_{water}}} = \frac{\boldsymbol{sens_{220kVp}}}{\boldsymbol{sens_{6MV}}} \tag{26}$$

It is reasonable that the sensitivity ratio between the energies is approximately similar to the ratio of the absorbed dose by the sample.

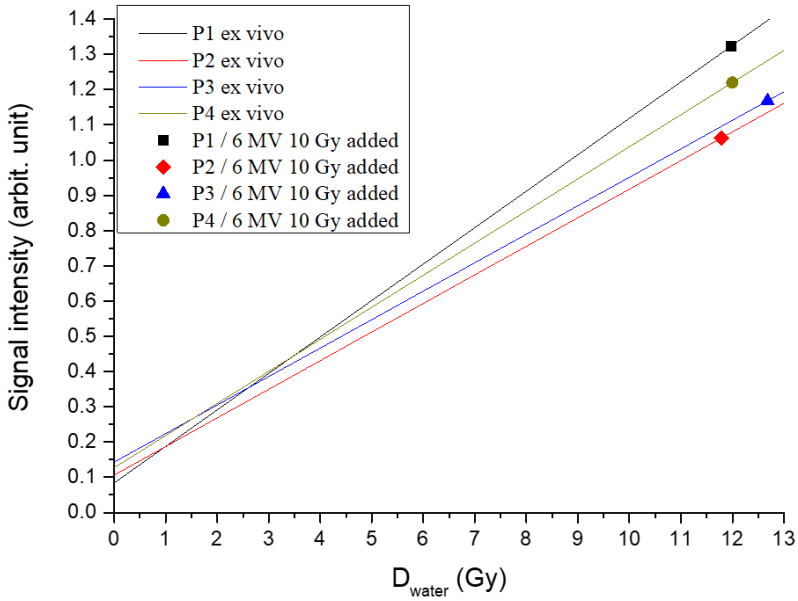

Figure 26 The signals measured from the teeth after the additional 6 MV irradiation was plotted on the dose-response curves of each tooth. The dose-response curves were the linear regression curves acquired from the data up to 10 Gy with the 220 kVp photon beam. The signals of the teeth were assessed with the water-absorbed doses, which are listed in Table 9.

Table 9 Dose assessment results of the teeth after further 10 Gy with the 6 MV X-ray beam. Only additional signal intensities exceeding that of the 10 Gy on the calibration curves were assessed as the water-absorbed dose.

	P1	P2	P3	P4
Assessed dose (Gy)	1.98	1.78	2.68	2.00
Mean assessed dose (Gy)	2.11			

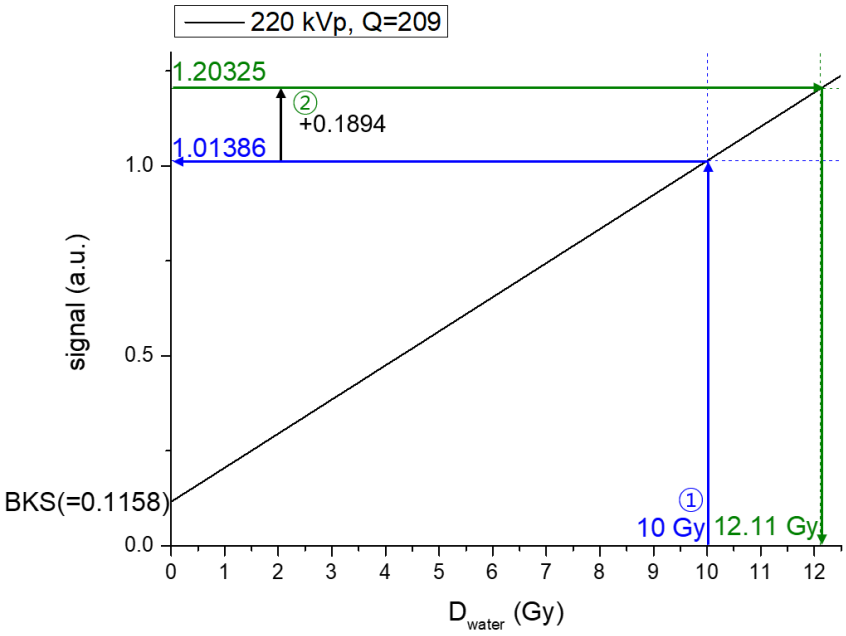

Figure 27 Visualization of the increased signal by the additional 6 MV irradiation shown on the dose-response curve acquired using 220 kVp beam.

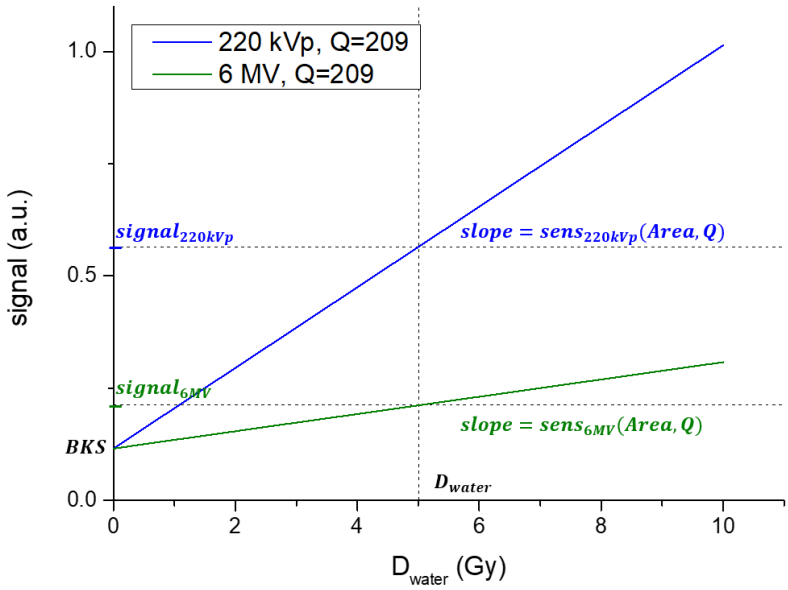

Figure 28 Viewpoint of the sensitivity in both energies, 220 kVp and 6 MV. Because the same water-absorbed dose increases different amounts of the signal in both energies, it is appropriate for the sensitivity become different in both energies. Consequently, the slope of the dose-response curve is different for both energies.

3.4.2. Verification Through Monte Carlo Simulation

The sensitivity ratio, which is approximately similar to the ratio of the absorbed dose to the tooth enamel is verified through the Monte Carlo calculation. The MCNP simulation was performed to calculate the absorbed dose to the tooth enamel.

First, the calculation was performed using the 220 kVp photon energy with the mimicked irradiation geometry used for the 220 kVp beam irradiation (Figure 19 (a)). To compare the absorbed dose to water, similar to the experiment, the sample material was changed to water after the calculation of the tooth enamel. The calculated results were;

$$\boldsymbol{d_{220kVp,\,enamel}} = \frac{D_{220kVp,\,enamel}}{(\#of\ photon)_{220kVp}} = 1.68 \times 10^{-4}\ [MeV \cdot g^{-1}] \tag{27}$$

(0.10% error)

$$\boldsymbol{d_{220kVp,\,water}} = \frac{D_{220kVp,\,water}}{(\#of\ photon)_{220kVp}} = 4.09 \times 10^{-5}\ [MeV \cdot g^{-1}] \tag{28}$$

(0.11% error)

$$\frac{\boldsymbol{d_{220kVp,\,enamel}}}{\boldsymbol{d_{220kVp,\,water}}} = \frac{\frac{D_{220kVp,\,enamel}}{(\#of\ photon)_{220kVp}}}{\frac{D_{220kVp,\,water}}{(\#of\ photon)_{220kVp}}} = \frac{D_{220kVp,\,enamel}}{D_{220kVp,\,water}} = \frac{1.68\times10^{-4}}{4.09\times10^{-5}} = \mathbf{4.10} \tag{29}$$

where $\boldsymbol{d_E}$ was the absorbed dose per photon history used in the Monte Carlo simulation.

The same procedure was followed for the 6 MV beam only changing the beam geometry and the energy spectrum (Figure 19 (b));

$$\boldsymbol{d_{6MV,\,enamel}} = \frac{D_{6MV,\,enamel}}{(\#of\ photon)_{6MV}} = 3.92 \times 10^{-4}[MeV \cdot g^{-1}] \tag{30}$$

(0.07% error)

$$\boldsymbol{d_{6MVp,\,water}} = \frac{D_{6MV,\,water}}{(\#of\ photon)_{6MV}} = 4.20 \times 10^{-4}\ [MeV \cdot g^{-1}] \tag{31}$$

(0.10% error)

$$\frac{\boldsymbol{d_{6MV,\,enamel}}}{\boldsymbol{d_{6MV,\,water}}} = \frac{\frac{D_{6MV,\,enamel}}{(\#of\ photon)_{6MV}}}{\frac{D_{6MV,\,water}}{(\#of\ photon)_{6MV}}} = \frac{D_{6MV,\,enamel}}{D_{6MV,\,water}} = \frac{3.92 \times 10^{-4}}{4.20 \times 10^{-4}} = \mathbf{0.933} \tag{32}$$

From the results of both energies, the sensitivity ratio, $\frac{\boldsymbol{sens_{220kVp}}}{\boldsymbol{sens_{6MV}}}$ was calculated as follows;

$$\left[\frac{\boldsymbol{d_{220kVp,\,enamel}}}{\boldsymbol{d_{220kVp,\,water}}}\right] \Big/ \left[\frac{\boldsymbol{d_{6MV,\,enamel}}}{\boldsymbol{d_{6MV,\,water}}}\right] = \left[\frac{D_{220kVp,\,enamel}}{D_{220kVp,\,water}}\right] \Big/ \left[\frac{D_{6MV,\,enamel}}{D_{6MV,\,water}}\right] = \frac{D_{220kVp,\,enamel}}{D_{6MV,\,enamel}} \cong \frac{\boldsymbol{sens_{220kVp}}}{\boldsymbol{sens_{6MV}}} = \frac{\mathbf{4.10}}{\mathbf{0.933}} = \mathbf{4.39} \tag{33}$$

Comparing the experimental results of 4.743, the calculated sensitivity ratio had a close value with a 7.4% error. It confirmed that the experimental results of the sensitivity ratio could be applied to the dose assessment by the 6 MV photon beam irradiation.

3.5. Measurement of Post-Radiotherapy Patients

The measurements from two post-radiotherapy patient volunteers were assessed for the dose estimation. From the volunteers, the EPR spectra were first measured from one of their maxillary incisors. Next, the S_{11} parameters were measured for the Q factor calculation. During this procedure, the volunteers maintained the same posture to that of the EPR measurements. Lastly, photographs of the measured teeth were taken to assess the size of the tooth for geometric correction. The acquired data are listed in Table 10.

The dose was estimated on the dose-response curve reconstructed with the Q factor of each patient using the relationship of the Q factor with the sensitivity and the background signal. For the Q factor measured from patient 1, the sensitivity and background signal were calculated as 0.05126 and 0.04699, respectively. From patient 2, they were 0.03945 and 0.02598, respectively (Figure 29, Table 11).

These calculated sensitivity was based on the normalized k_{geo}. Because the measured EPR signal was not corrected for the tooth area effect, the calculated sensitivity should be divided by k_{geo} for application in the assessment of a specific tooth. In this case;

$$\boldsymbol{sens_{patient1,\,220kVp}} = \frac{\boldsymbol{sens_{220kVp}}}{\boldsymbol{k_{geo,patient1}}} \tag{34}$$

$$\boldsymbol{sens_{patient2,\,220kVp}} = \frac{\boldsymbol{sens_{220kVp}}}{\boldsymbol{k_{geo,patient2}}} \tag{35}$$

The calculated values are listed in Table 11.

The EPR signals assessed were acquired from the patients' teeth irradiated under the 6 MV beam at the hospital. Because the calculated sensitivities, $\boldsymbol{sens_{patient,\,220kVp}}$, were based on the 220 kVp beam, they should be converted to $\boldsymbol{sens_{patient,\,6MV}}$ for use in the patients' dose assessment.

$$\boldsymbol{sens_{6MV}} = \frac{\boldsymbol{sens_{220kVp}}}{\boldsymbol{sens_{220kVp}/sens_{6MV}}} = \frac{\boldsymbol{sens_{220kVp}}}{\boldsymbol{4.743}} \tag{36}$$

where the value 4.743 of $\frac{\boldsymbol{sens_{220kVp}}}{\boldsymbol{sens_{6MV}}}$ was experimentally acquired. The values of $\boldsymbol{sens_{patient1,6MV}}$ and $\boldsymbol{sens_{patient2,6MV}}$ were 0.00744 and 0.00562, respectively. The dose-response curve for patient 1, and patient 2 are shown in Figure 30. The dose-response curve with the sensitivity based on the 220 kVp (blue) were converted to the dose-response curve to assess the 6 MV (green).

The measured EPR signals were assessed using this dose-response curve with the 6 MV sensitivity for each patient. The assessed doses were 2.69, and 12.7 Gy from patients 1 and 2, respectively.

Table 10 Q factor measured from in-vivo subjects treated with total body irradiation

	Patient 1	Patient 2
Q factor	98	64
Height of tooth (mm)	7.0	7.2
Width of tooth (mm)	10.1	9.7
Enamel area (mm^2)	70.7	69.5
k_{geo}	1.452	1.481

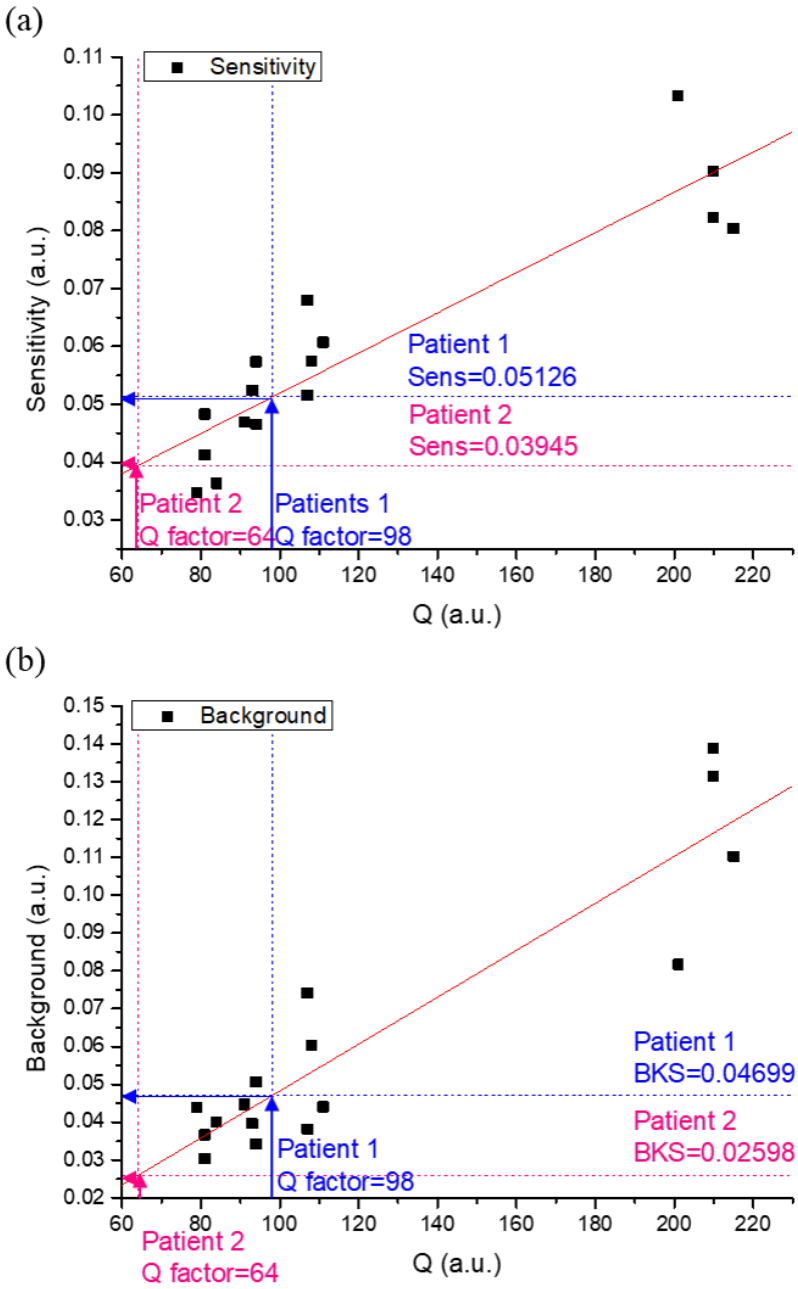

Figure 29 Procedure to calculate the sensitivity and background signal for volunteers' Q factors. (a) Sensitivity and (b) background signal

Table 11 Sensitivity and background signal calculated from Q factor measured from patient 1 and patient 2

	Patient 1	Patient 2
sens_{220kVp}	0.05126	0.03945
BKS	0.04699	0.02598
$\mathrm{sens}_{patient,220kVp}$	0.03529	0.02664
$\mathrm{sens}_{patient,6MV}$	0.00744	0.00562

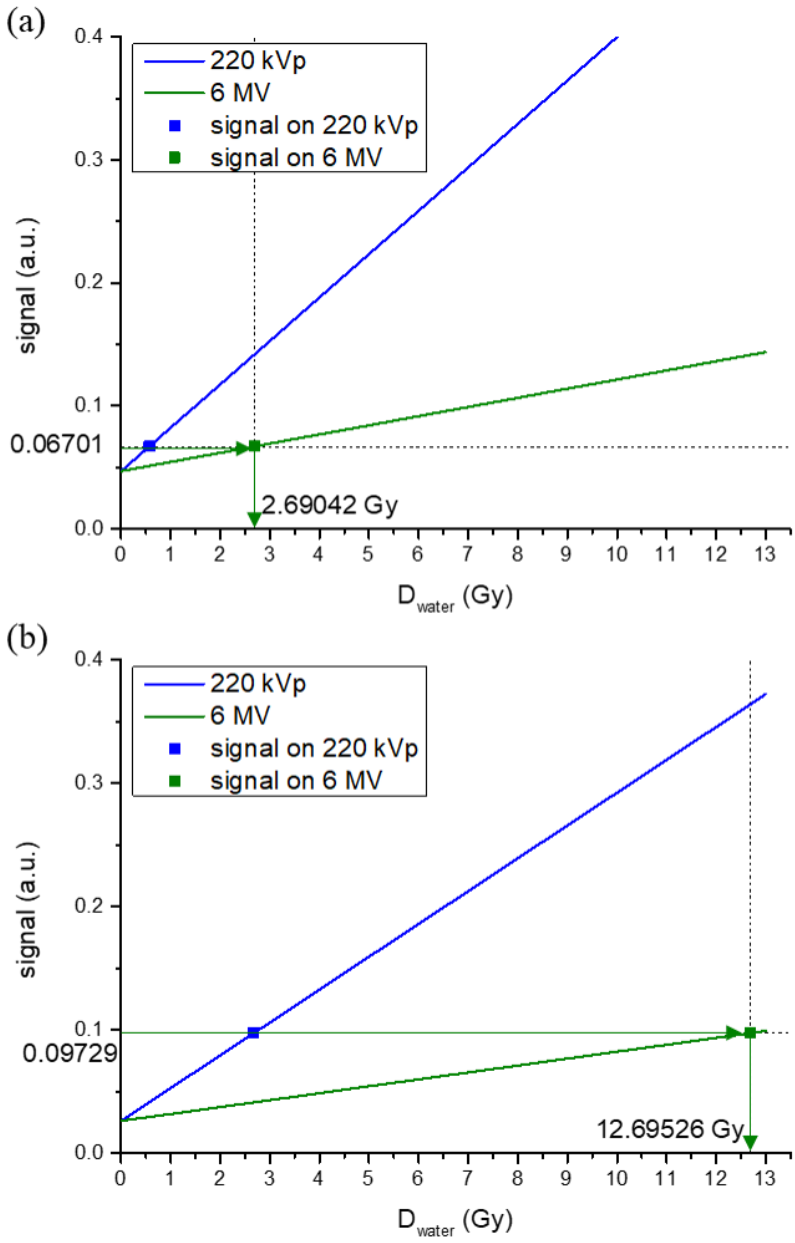

Figure 30 Dose-response curve of post-treatment patients generated using Q factor. Dose-response curve with sensitivity calculated for the 220 kVp (blue) was converted to that of the 6 MV (green).

3.6. Effect of Irradiation Geometry of Post-Radiotherapy Patients

Up to this part, the EPR signals measured from the teeth of the post-radiotherapy patients were assessed based on the water-absorbed dose to the tooth. From the American Association of Physics in Medicine (AAPM) protocol of TBI treatment, the prescription dose was determined based on the absorbed dose on the midpoint at the level of the umbilicus, which is far from the tooth [42]. For the TBI treatment that is mainly a procedure before bone marrow transplant, the radiation dose is intended to be transferred uniformly along the longitudinal body axis. Therefore, ideally, the equivalent dose is transferred to the longitudinal axis of the body. Assuming that the longitudinal axis of the body received an equivalent dose, the center of the head also received the same dose.

For the verification of the relative dose transferred to the location of the tooth compared to the axis of the body, the Monte Carlo simulation was performed (Figure 31). The MCNP Monte Carlo code was used.

A head-sized cylindrical phantom composed of water was modeled for the simulation assuming that it was the head. The height and diameter were 15 cm. For the location of the tooth, a small water sphere with a 1.5 mm diameter was placed at the midlevel height of the head phantom. Considering the thickness of the lip, the absorbed dose to the small sphere was estimated at various horizontal locations from the shallow depth (1 mm from the surface) to the center of the cylindrical head phantom (7.5 cm from the surface).

Because the post-radiotherapy patients were treated with a bilateral 6 MV photon beam, the photon beam with the energy spectrum of the clinical linear accelerator was irradiated from both sides. The water-absorbed dose of the tooth location was compared to that of the center location of the head cylinder

The results are listed in Table 12. Assuming the thickness of

the lip as 1 cm, the water-absorbed dose transferred to the location of the tooth is 110.8%. In the case of the prescription dose 4 and 12 Gy, the tooth received a 4.43 and 13.29 Gy water-absorbed dose, respectively (Table 13). Compared to these values, the assessed dose from the EPR measurements were underestimated by 39% from patient 1 and overestimated by 4% from patient 2.

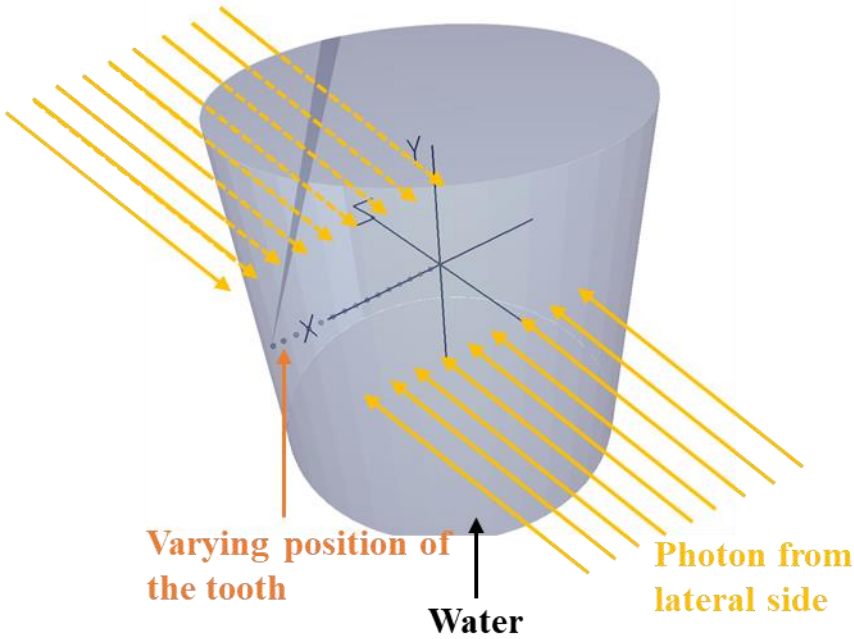

Figure 31 Geometry used for Monte Carlo calculation to verify the absorbed dose to the location of the tooth. For the head, a cylindrical water phantom with a 15 cm diameter and 15 cm height was used. To estimate the dose to the tooth location, a sphere with a 1.5 mm diameter was located on the middle level of the cylindrical phantom. The location of the small sphere was changed from a 0.1 mm depth to the center of the cylinder from the surface. A bilateral 6 MV photon beam was used to simulate the treatment situation.

Table 12 Calculated results of Monte Carlo simulation.

Distance from the surface (cm)	Water-absorbed dose (MeV/g)	Error (%)	Relative dose compared to the center (%)
7.5	1.58E-04	0.0078	100
7	1.61E-04	0.0078	102.0
6.5	1.59E-04	0.0078	100.5
6	1.60E-04	0.0078	101.1
5.5	1.62E-04	0.0077	102.4
5	1.60E-04	0.0078	101.4
4.5	1.61E-04	0.0077	102.2
4	1.62E-04	0.0077	102.7
3.5	1.63E-04	0.0077	103.3
3	1.64E-04	0.0077	103.7
2.5	1.69E-04	0.0076	106.8
2	1.68E-04	0.0076	106.6
1.5	1.69E-04	0.0075	107.2
1	1.75E-04	0.0075	110.8
0.5	1.84E-04	0.0073	116.2
0.1	1.92E-04	0.0071	121.7

Table 13 Comparison of the assessed results from the EPR measurements (assessed D_{water} from measurement) with the estimated results from the Monte Carlo calculation (D_{water} from Monte Carlo calculation). The water-absorbed dose from the Monte Carlo calculation was calculated from the relative ratio in Table 12 with the prescription dose.

Subject	Assessed D_{water} from measurement (Gy)	Prescription dose (Gy)	D_{water} from Monte Carlo calculation (Gy)	Relative error
Patient 1	2.69	4	4.43	-39%
Patient 2	12.7	12	13.29	4%

3.7. Inverse Prediction for Dose Estimation

The dose estimation used in the method uses the inverse dose prediction from the signal amplitude. Therefore, the performance of the dose estimation system was assessed from the viewpoint of the inverse prediction. The standard error of inverse prediction (SEIP) was evaluated for the dose assessment.

The SEIP was evaluated for each situation – without the in vivo phantom (ex vivo), −2 mm depth, 0 mm depth, and +2 mm depth with the in vivo phantom; these are listed in Table 14. The CI was calculated from the evaluated SEIP [43]. The SEIP values were calculated as 0.53 Gy for ex vivo, 0.59 Gy for the depth of −2 mm, 0.53 for the depth of 0 mm, and 0.78 Gy for the depth of +2 mm. The average SEIP for the four situations was 0.61 Gy. From the SEIP values, 95% and 75% CI levels were also calculated.

The method for calculating the dose−response curve for the Q factor was evaluated through SEIP. For this evaluation, the Q−factor generated dose−response curve was first acquired for the Q factor measured from the tooth and the pseudo−in−vivo phantom. SEIP was calculated between the geometry corrected data and Q factor generated curve. The results are listed in Table 15.

With this error, another error source is identified in the aforementioned Q factor distribution (Table 8). From this Q factor distribution error, the possible error in the patient dose assessments could be calculated. The results from patient 1 had an error in the estimated dose, which was calculated at Q factor 98 and 2.69 Gy. The error was 0.42 Gy with 95% CI, and 0.24 Gy with 75% CI. For patient 2, it was calculated at Q factor 64 and 12.7 Gy. The error was 2.53 Gy with 95% CI, and 1.42 Gy with 75% CI.

Table 14 SEIP evaluated for each in vivo phantom depth.

	Ex vivo	In vivo phantom −2 mm	In vivo phantom 0 mm	In vivo phantom +2 mm
SEIP (Gy)	0.53	0.59	0.53	0.78
95% CI (Gy)	1.05	1.15	1.04	1.53
75% CI (Gy)	0.62	0.68	0.61	0.90

Table 15 SEIP for the Q factor generated dose−response curve

	SEIP (Gy)	95% CI (Gy)	75% CI (Gy)	Mean SEIP (Gy)
P1	0.80	1.59	0.93	0.58
P2	0.75	1.49	0.87	
P3	0.43	0.86	0.50	
P4	0.34	0.68	0.39	
P1 pseudo in vivo depth −2 mm	1.23	2.43	1.42	0.74
P2 pseudo in vivo depth −2 mm	0.67	1.33	0.78	
P3 pseudo in vivo depth −2 mm	0.56	1.11	0.65	
P4 pseudo in vivo depth −2 mm	0.49	0.97	0.56	
P1 pseudo in vivo depth 0 mm	0.77	1.53	0.89	0.52
P2 pseudo in vivo depth 0 mm	0.52	1.03	0.60	
P3 pseudo in vivo depth 0 mm	0.44	0.88	0.51	
P4 pseudo in vivo depth 0 mm	0.36	0.71	0.42	
P1 pseudo in vivo depth 2 mm	0.47	0.94	0.55	0.86
P2 pseudo in vivo depth 2 mm	0.70	1.39	0.81	
P3 pseudo in vivo depth 2 mm	1.22	2.42	1.41	
P4 pseudo in vivo depth 2 mm	1.07	2.12	1.23	
Total mean	0.68	1.34	0.78	

3.8. Discussion on Error Level of Post-Treatment Patients

The dosimetric performance for the assessed dose from the patient measurements had an error compared to the estimated absorbed dose received by their teeth (Table 13). From patient 1 who had received a 4 Gy prescription dose, 2.69 Gy was assessed from the EPR measurement. The discrepancy from the expected received dose was 1.74 Gy, which was a 39% error. From patient 2, the discrepancy was 0.59 Gy, which was a 4% error. Compared to the SEIP, which had a standard error in the assessment of the EPR signal to the water−absorbed dose, the error in patient 1 was relatively large. The discrepancy exhibited by patient 2 was in the range of expectation compared to the total mean value of the SEIP although it was still high compared to that of the ex vivo conditions −2 mm depth or 0 mm depth.

One of the reasons for the high discrepancy observed in the patient measurements is the movement of the patient during the measurement. During the in vivo measurement, although we tried to control the patients' movement, the breathing significantly disrupted the coupling status of the resonator. Therefore, we ordered patients to take a breath during the measurement. Even with this, the disturbance of the coupling status appears after one sweep of the spectrum measurements. Even the first sweep spectrum was affected by the disturbance.

To compensate for the disturbance by movement during the in vivo measurement, studies developed a compensating circuitry, which controlled the frequency of the system following the changing coupling status of the resonator [12]. This would be the required study for the future work in the in vivo tooth dosimetry.

3.9. Q Factor Correction: Another Method to Compensate for the Q Factor Effect

Another method used to reflect the effect of the Q factor was considered. There were limitations in the method previously described. The limitations were found in the relationships of the Q factor with the dosimetric sensitivity and background signal. The dose-response curve is calculated from the regression curves of the Q factor relationships. The Q factor distribution where the regression curve was plotted had a blank space in the range between 111 and 210. Plotting linear regression lines over that blank range can be criticized for its logical weakness. Although the regression lines were drawn over the wide Q factor range from 79 to 215, the Q factor measured from in the vivo volunteers was distributed from 60 to 101.

Considering the purpose of the method reflecting the quality factors, the regression curve over the wide range may have a different tendency from the actual in vivo range. The regression curve for the Q factor relationships can be drawn only for the range where the pseudo-in-vivo phantom was used. However, in that case, the linear regression curve has a very low linear relationship. The coefficient of determination, R^2, is 0.662 for the dosimetric sensitivity and 0.3019 for the background signal.

Another method for the estimation of the absorbed dose reflecting the Q factor is based on the theoretical expression of the EPR signal. The EPR signal is expressed as

$$\text{EPR signal} = \chi\ \eta\ \mathrm{Q}\sqrt{PZ_0} \tag{37}$$

where χ is the magnetic susceptibility of the sample tooth, η is the filling factor, Q is the Q factor, P is the incident microwave power of the resonator, and Z_0 is the characteristic impedance of the transmission line of the resonator [37]. By the equation, the EPR signal is directly proportional to the Q factor. Although the previous method was also based on the fact that the EPR signal is

proportional to the Q factor, there was an intercept in its relationships. In that method, even with a zero Q factor, the EPR signal did not become zero.

Naturally, the signal becomes zero at zero Q factor considering the definition of the Q factor:

$$\text{Q factor} = \frac{Energy\ stored\ in\ the\ resonator}{Energy\ dissipated\ in\ the\ resontor} \tag{38}$$

If there is no stored energy (Q factor=0), then the signal becomes zero.

In the equation of the EPR signal, there are other comprising components. The magnetic susceptibility is proportional to the number of spins in the sample. In the in vivo tooth dosimetry, it is proportional to the absorbed dose of the sample tooth [36]. The filling factor of the resonator is determined by the relative location of the resonator and sample tooth. The relative location of the tooth and resonator was carefully adjusted to avoid differing between the teeth. There was an inevitable difference in the size of the teeth, which was moderated with the geometric correction using the tooth enamel area. The power incident to the resonator was not changed during the measurements. Consequently, it is roughly assumed that the EPR signal is directly proportional to the Q factor. If there is a difference in the Q factor between the measurement conditions, the effect of the Q factor can be compensated with the normalization of the Q−factor;

$$(EPR\ signal\ normlized\ with\ Q\ factor) = \frac{\text{EPR signal}}{Q} \tag{39}$$

With this method, the difference in the dosimetric sensitivity due to the Q factor difference is considered to be corrected.

3.9.1. Results of Q Factor Correction

For the Q factor correction, the measured EPR signals are first normalized with the Q factor for each sample;

$$\text{signal}_{Q\ norm} = \frac{signal}{Q} \tag{40}$$

The results of the Q factor correction are shown in Figure 32. The SEIP and its CI are listed in Table 16. The scattered data points are concentrated with the normalization of the correction. After geometric correction, SEIP decreased to 0.64 Gy. The 95% CI and 75% CI were 1.26 and 0.74 Gy, respectively.

The EPR spectra measured from the post-radiotherapy patients were assessed using this method. The results are listed in Table 17. The assessed water-absorbed dose from the teeth of patients 1 and 2 were 2.73 and 12.53 Gy, respectively, and the relative differences from the estimated irradiated dose were 38% and 6%, respectively. The discrepancies in the assessed dose from the estimated irradiated dose were 1.70 Gy and 0.76 Gy. Assuming that the treated dose was transferred as a prescription dose, the dose assessed from patient 1 was in the range of 99.2% CI, whereas that from patient 2 was included in the range of 77% CI, which was not shown in the table.

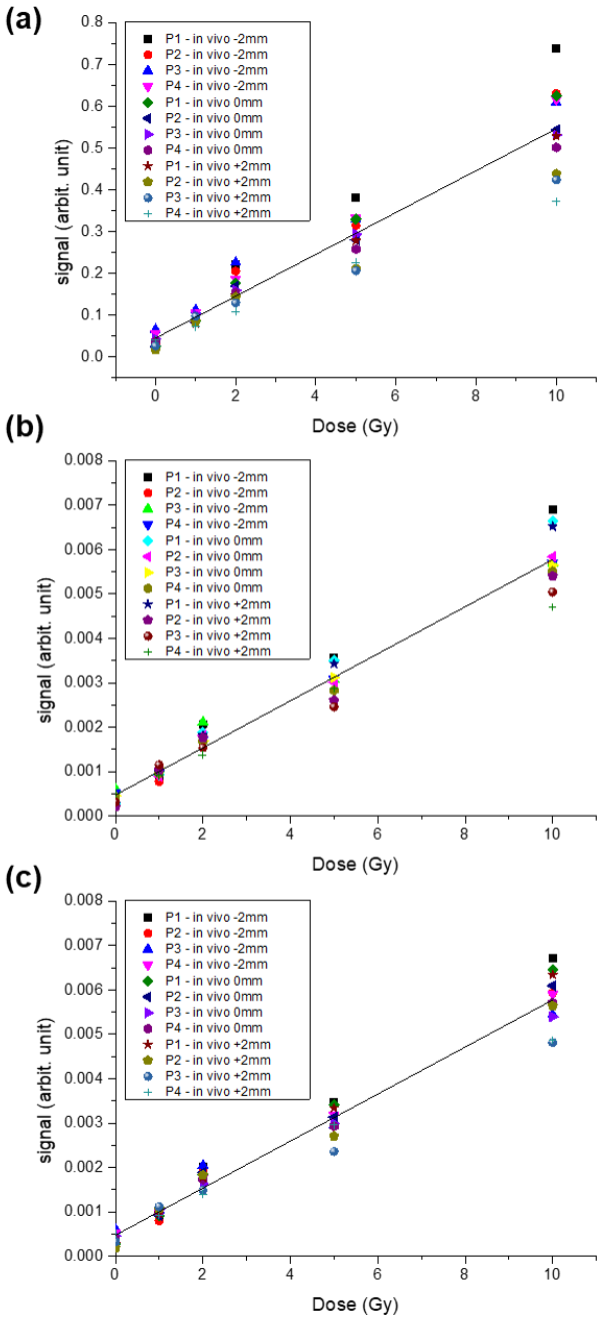

Figure 32 Dose-response curves and data points drawn based on (a) experimental raw data (b) Q factor corrected data and (c) Data geometric corrected after Q factor correction.

Table 16 SEIP and confidence interval (CI) for Q factor correction method

	Raw signal	Q factor corrected	Geometric corrected (with QC)
SEIP (Gy)	1.11	0.68	0.64
95% CI (Gy)	2.20	1.35	1.26
75% CI (Gy)	1.28	0.79	0.74

Table 17 Post-radiotherapy patient dose assessment

	Estimated irradiated dose (Gy)	Assessed dose from measurement (Gy)	Relative difference	Dose discrepancy (Gy)
Patient 1	4.43	2.73	−38%	−1.70
Patient 2	13.29	12.53	−6%	−0.76

3.9.2. Comparison of Two Q Factor Reflection Methods

While the level of discrepancy was not so different in the two methods, there were cons and pros in each method.

The first method of calculating the dose-response curve for an arbitrary Q factor is based on the trends of the Q factor relationships. It is more intuitive to consider the sensitivity and background signal changes following the Q factor. However, the relationships were based on the weak correlation of the Q factor distribution. Moreover, the Q factor distribution dispersed in a wide range than that required for the in vivo measurement. The in vivo Q factor range concentrated on low Q factors, whereas the regression curve used up higher Q factors. This was due to the low correlation at the low Q factor range.

Compared to this, the second method used only a low Q factor range. The data observed under the in vivo circumstances were used. This method was based on the theoretical base of the EPR signal components. It was more convenient for application. However, this method did not explain the existence of the noise signal in the background signal generated from the device itself.

Chapter 3. Conclusion

A magnet for in vivo tooth dosimetry was successfully developed and verified through spectrum acquisition using irradiated teeth. The magnet was lighter than the benchmarked model; thus, it exhibits better mobile functionality than conventional models.

With the developed magnet and our previously developed CW EPR spectrometer, a tooth dosimetry study was performed for in vivo dose measurement.

The Q factor controllable pseudo-in-vivo phantom was proposed and applied to the actual dose assessment of patients in-vivo. From the several pre-acquired dose-response curves, the patient-adaptive calibration curve was acquired using the Q factor measured from the patients. Based on the calibration curves, and further calculation, the irradiation doses of the patients during the treatment were closely estimated.

Bibliography

[1] S. Akita, Treatment of radiation injury, Advances in wound care, 3 (2014) 1-11, https://doi.org/10.1089/wound.2012.0403.
[2] M. Berger, D. Christensen, P. Lowry, O. Jones, A. Wiley, Medical management of radiation injuries: current approaches, Occupational Medicine, 56 (2006) 162-172, https://doi.org/10.1093/occmed/kql011.
[3] T.L. Ryan, M.B. Escalona, T.L. Smith, J. Albanese, C.J. Iddins, A.S. Balajee, Optimization and validation of automated dicentric chromosome analysis for radiological/nuclear triage applications, Mutation Research/Genetic Toxicology and Environmental Mutagenesis, 847 (2019) 503087, https://doi.org/10.1016/j.mrgentox.2019.503087.
[4] A. Lund, M. Shiotani, Applications of EPR in radiation research, Springer, 2014,
[5] B.B. Williams, A.B. Flood, I. Salikhov, K. Kobayashi, R. Dong, K. Rychert, G. Du, W. Schreiber, H.M. Swartz, In vivo EPR tooth dosimetry for triage after a radiation event involving large populations, Radiation and environmental biophysics, 53 (2014) 335-346, https://doi.org/10.1007/s00411-014-0534-9.
[6] A. Ivannikov, E. Gaillard-Lecanu, F. Trompier, V. Stepanenko, V. Skvortsov, N. Borysheva, D. Tikunov, D. Petin, Dose reconstruction by EPR spectroscopy of tooth enamel: application to the population of Zaborie village exposed to high radioactive contamination after the Chernobyl accident, Health physics, 86 (2004) 121-134, https://doi.org/10.1097/00004032-200402000-00002.
[7] A. Romanyukha, D. Regulla, E. Vasilenko, A. Wieser, South Ural nuclear workers: Comparison of individual doses from retrospective EPR dosimetry and operational personal monitoring, Applied Radiation and Isotopes, 45 (1994) 1195-1199, https://doi.org/10.1016/0969-8043(94)90036-1.
[8] N. Nakamura, C. Miyazawa, S. Sawada, M. Akiyama, A. Awa, A close correlation between electron spin resonance (ESR) dosimetry from tooth enamel and cytogenetic dosimetry from lymphocytes of Hiroshima atomic-bomb survivors, International journal of radiation biology, 73 (1998) 619-627, https://doi.org/10.1080/095530098141870.
[9] W. Schreiber, S.V. Petryakov, M.M. Kmiec, A.B. Flood, H.M. Swartz, P.E. Schaner, B.B. Williams, In Vivo CW-EPR Spectrometer Systems for Dosimetry and Oximetry in Preclinical and Clinical Applications, Applied Magnetic Resonance, (2021) 1-21, https://doi.org/10.1007/s00723-021-01382-7.
[10] J. Guo, X. Luan, Y. Tian, L. Ma, X. Bi, J. Zou, G. Dong, Y. Liu, Y. Li, J. Ning, The design of X-band EPR cavity with narrow detection aperture for in vivo fingernail dosimetry after accidental exposure to ionizing radiation, Scientific Reports, 11 (2021) 1-8, https://doi.org/10.1038/s41598-021-82462-3.
[11] J. Zou, J. Guo, L. Ma, G. Dong, J. Cong, Y. Liu, Y. Tian, K. Wu, A normalization method of the volume and geometry of tooth for X-band in

vivo EPR dosimetry, Appl Radiat Isot, 149 (2019) 123-129, https://doi.org/10.1016/j.apradiso.2019.04.023.
[12] H. Hirata, T. Walczak, H.M. Swartz, Electronically tunable surface-coil-type resonator for L-band EPR spectroscopy, Journal of magnetic Resonance, 142 (2000) 159-167, https://doi.org/10.1006/jmre.1999.1927.
[13] C.Z. Cooley, M.W. Haskell, S.F. Cauley, C. Sappo, C.D. Lapierre, C.G. Ha, J.P. Stockmann, L.L. Wald, Design of sparse Halbach magnet arrays for portable MRI using a genetic algorithm, IEEE transactions on magnetics, 54 (2017) 1-12, https://doi.org/10.1109/TMAG.2017.2751001.
[14] M. Nakagomi, M. Kajiwara, J. Matsuzaki, K. Tanabe, S. Hoshiai, Y. Okamoto, Y. Terada, Development of a small car-mounted magnetic resonance imaging system for human elbows using a 0.2 T permanent magnet, Journal of Magnetic Resonance, 304 (2019) 1-6, https://doi.org/10.1016/j.jmr.2019.04.017.
[15] H.M. Swartz, B.B. Williams, B.I. Zaki, A.C. Hartford, L.A. Jarvis, E.Y. Chen, R.J. Comi, M.S. Ernstoff, H. Hou, N. Khan, Clinical EPR: unique opportunities and some challenges, Academic radiology, 21 (2014) 197-206, https://doi.org/10.1016/j.acra.2013.10.011.
[16] B.B. Williams, R. Dong, A.B. Flood, O. Grinberg, M. Kmiec, P.N. Lesniewski, T.P. Matthews, R.J. Nicolalde, T. Raynolds, I.K. Salikhov, A deployable in vivo EPR tooth dosimeter for triage after a radiation event involving large populations, Radiation measurements, 46 (2011) 772-777, https://doi.org/10.1016/j.radmeas.2011.03.009.
[17] H. Sato-Akaba, Y. Okada, K. Tsuji, M.C. Emoto, H.G. Fujii, Design and Fabrication of Compact Arrayed Magnet for Biological EPR Imaging, Applied Magnetic Resonance, 52 (2021) 1017-1029, https://doi.org/10.1007/s00723-020-01256-4.
[18] K. Sirota, Y. Twig, A. Blank, Pulsed electron spin resonance ex situ probe for tooth biodosimetry, Applied Magnetic Resonance, 44 (2013) 671-689, https://doi.org/10.1007/s00723-012-0435-5.
[19] H. Woflson, R. Ahmad, Y. Twig, B. Williams, A. Blank, A magnetic resonance probehead for evaluating the level of ionizing radiation absorbed in human teeth, Health physics, 108 (2015) 326-335, https://doi.org/10.1097/HP.0000000000000187.
[20] C. Bauer, H. Raich, G. Jeschke, P. Blümler, Design of a permanent magnet with a mechanical sweep suitable for variable-temperature continuous-wave and pulsed EPR spectroscopy, Journal of magnetic resonance, 198 (2009) 222-227, https://doi.org/10.1016/j.jmr.2009.02.010.
[21] G.A. Rinard, R.W. Quine, G.R. Eaton, S.S. Eaton, E.D. Barth, C.A. Pelizzari, H.J. Halpern, Magnet and gradient coil system for low-field EPR imaging, Concepts in Magnetic Resonance: An Educational Journal, 15 (2002) 51-58, https://doi.org/10.1002/cmr.10018.
[22] H. Sato-Akaba, H. Fujii, H. Hirata, Development and testing of a CW-EPR apparatus for imaging of short-lifetime nitroxyl radicals in mouse head, Journal of Magnetic Resonance, 193 (2008) 191-198, https://doi.org/10.1016/j.jmr.2008.04.035.
[23] C.P. Poole, Electron spin resonance: a comprehensive treatise on experimental techniques, (1996) 213, 214,

[24] P. Fattibene, F. Callens, EPR dosimetry with tooth enamel: a review, Applied Radiation and Isotopes, 68 (2010) 2033-2116, https://doi.org/10.1016/j.apradiso.2010.05.016.
[25] I. Salikhov, T. Walczak, P. Lesniewski, N. Khan, A. Iwasaki, R. Comi, J. Buckey, H. Swartz, EPR spectrometer for clinical applications, Magnetic Resonance in Medicine: An Official Journal of the International Society for Magnetic Resonance in Medicine, 54 (2005) 1317-1320, https://doi.org/10.1002/mrm.20689.
[26] W. Lee, J. Park, J. Jeong, E. Jeon, H.-E. Kim, S. Park, H. You, Analysis of the facial anthropometric data of Korean pilots for oxygen mask design, in: Proceedings of the Human Factors and Ergonomics Society Annual Meeting, SAGE Publications Sage CA: Los Angeles, CA, 2012, pp. 1927-1931, https://doi.org/10.1177/1071181312561282.
[27] D. Cai, L.-L. Huang, T. Liu, M. You, Determining Cockpit Dimensions and Associative Dimensions between Components in Cockpit of Ultralight Plane for Taiwanese, in: International Conference on Digital Human Modeling, Springer, 2009, pp. 365-374, https://doi.org/10.1007/978-3-642-02809-0_39.
[28] W. Lee, B. Lee, X. Yang, H. Jung, I. Bok, C. Kim, O. Kwon, H. You, A 3D anthropometric sizing analysis system based on North American CAESAR 3D scan data for design of head wearable products, Computers & Industrial Engineering, 117 (2018) 121-130, https://doi.org/10.1016/j.cie.2018.01.023.
[29] E.J. Dickinson, H. Ekström, E. Fontes, COMSOL Multiphysics®: Finite element software for electrochemical analysis. A mini-review, Electrochemistry communications, 40 (2014) 71-74, https://doi.org/10.1016/j.elecom.2013.12.020.
[30] R.C. Brandao, L.B. Brandao, Finishing procedures in orthodontics: dental dimensions and proportions (microesthetics), Dental Press J Orthod, 18 (2013) 147-174, https://doi.org/10.1590/s2176-94512013000500006.
[31] J.I. Park, K. Choi, C.U. Koo, J. Oh, H. Hirata, H.M. Swartz, S.J. Ye, Dependence of Radiation-induced Signals on Geometry of Tooth Enamel Using a 1.15 GHz Electron Paramagnetic Resonance Spectrometer: Improvement of Dosimetric Accuracy, Health Phys, 120 (2021) 152-162, https://doi.org/10.1097/HP.0000000000001292.
[32] B.D. Cullity, C.D. Graham, Introduction to magnetic materials, (2011) 497, https://doi.org/10.1002/9780470386323.ch14.
[33] B.B. Williams, R. Dong, R.J. Nicolalde, T.P. Matthews, D.J. Gladstone, E. Demidenko, B.I. Zaki, I.K. Salikhov, P.N. Lesniewski, H.M. Swartz, Physically-based biodosimetry using in vivo EPR of teeth in patients undergoing total body irradiation, International journal of radiation biology, 87 (2011) 766-775, https://doi.org/10.3109/09553002.2011.583316.
[34] K. Kobayashi, R. Dong, R.J. Nicolalde, P. Calderon, G. Du, B.B. Williams, H.M. Swartz, A.B. Flood, Development of a novel mouth model as an alternative tool to test the effectiveness of an in vivo EPR dosimetry system, Physics in Medicine & Biology, 63 (2018) 165002, https://doi.org/10.1088/1361-6560/aad518.
[35] H. Hirata, T. Walczak, H.M. Swartz, Characteristics of an electronically

tunable surface-coil-type resonator for L-band electron paramagnetic resonance spectroscopy, Review of Scientific Instruments, 72 (2001) 2839-2841,
[36] B.B. Williams, A. Sucheta, R. Dong, Y. Sakata, A. Iwasaki, G. Burke, O. Grinberg, P. Lesniewski, M. Kmiec, H.M. Swartz, Experimental procedures for sensitive and reproducible in situ EPR tooth dosimetry, Radiation measurements, 42 (2007) 1094-1098, https://doi.org/10.1016/j.radmeas.2007.05.001.
[37] G.R. Eaton, S.S. Eaton, D.P. Barr, R.T. Weber, Quantitative Epr, Springer Science & Business Media, 2010,
[38] M. Robinson, M. Richardson, J. Green, A. Preece, New materials for dielectric simulation of tissues, Physics in Medicine & Biology, 36 (1991) 1565,
[39] K. Choi, C. Koo, J. Oh, J.I. Park, H. Hirata, S.-J. Ye, Development of Electron Paramagnetic Resonance Magnet System for In Vivo Tooth Dosimetry, Concepts in Magnetic Resonance Part B, Magnetic Resonance Engineering, 2022 (2022), https://doi.org/10.1155/2022/7332324.
[40] A. Iwasaki, T. Walczak, O. Grinberg, H.M. Swartz, Differentiation of the observed low frequency (1200 MHz) EPR signals in whole human teeth, Applied radiation and isotopes, 62 (2005) 133-139, https://doi.org/10.1016/j.apradiso.2004.08.038.
[41] A. Ivannikov, D. Tikunov, N. Borysheva, F. Trompier, V. Skvortsov, V. Stepanenko, M. Hoshi, Calibration of EPR signal dose response of tooth enamel to photons: experiment and Monte Carlo simulation, Radiation protection dosimetry, 108 (2004) 303-315, https://doi.org/10.1093/rpd/nch040.
[42] J. Dyk, J. Galvin, G. Glasgow, E. Podgorsak, AAPM Report No. 17: The Physical Aspects of Total and Half Body Photon Irradiation, American Association of Physicists in Medicine, (1986), https://doi.org/10.37206/16.
[43] P. Fattibene, A. Wieser, E. Adolfsson, L. Benevides, M. Brai, F. Callens, V. Chumak, B. Ciesielski, S. Della Monaca, K. Emerich, The 4th international comparison on EPR dosimetry with tooth enamel: Part 1: Report on the results, Radiation Measurements, 46 (2011) 765-771,

List of Abbreviations

ABBREVIATION	DESCRIPTION
^{15}N-PDT	4-oxo-2,2,6,6-tetramethylpiperidine-d_{16}–1-^{15}N-1-oxyl
AAPM	American Associaion of Physics in Medicine
AC	Alternating current
CAESAR	Civilian American and European Surface Anthropometry Resource
CI	Confidence interval
CW	Continuous wave
DC	Direct current
DSV	Diameter of a spherical volume
EMF	Electromotive force
EPR	Electron paramagentic resonance
FEM	Finite element method
NdFeB	$Nd_2Fe_{14}B$
NMR	Nuclear magnetic resonance
PM	Permanent magnet
RIS	Radiation-induced signal
SEIP	Standard error of inverse prediction
TBI	Total body irradiation

Abstract in Korean

대규모 방사선 사고 상황에서 부상자/환자 분류를 위한 목적에 있어 체내 전자상자성공명 치아 선량평가는 피폭된 환자를 신속하게 구분하는데 유일하면서도 유용한 방법이다. 방사선사고 대응에 있어서 사고현장으로 이동하여 사용할 수 있는 이동성은 중요한 요소로 작용한다. 전자상자성공명 분광계의 가장 무거운 부분은 자석이며, 이의 경량화 및 체내측정 최적화를 통해 치아 선량평가를 사고 현장에서 수행할 수 있도록 개발하는 것이 본 논문의 목적이다. 또한 이는 종합적으로 전자상자성공명 분광계 전체를 개발하고자 했던 지난 연구 프로젝트의 일환으로 수행되었다.

논문의 두번째 부분에서는 새로이 개발된 자석을 이용하여 체내 치아 선량평가를 수행한 내용이 설명된다. 발치된 치아로부터 선량-반응 곡선을 얻을 수 있지만 체내 환경에서 측정되는 선량-반응 정보는 선량 민감도가 다르기에 추가로 체내에서의 측정이 필요하다. 이 선량 민감도의 차이는 주로 Q 팩터의 차이를 통해 나타나게 된다. 방사선을 조사받지 않은 지원자들의 구강 내 치아로부터 체내 Q 팩터에 개인차가 있음을 확인하였다. 이 개인차를 반영하기 위한 새 방법이 본 논문에서 제안되었다. 논문에서 제작, 제안한 의사 체내 팬텀이 이 방법에서 중요한 역할을 하였다. Q 팩터를 체내 Q 팩터의 범위 내에서 의도적으로 변화시키는 것이다.

논문 전체에 걸쳐 새로 개발된 자석의 성능을 세 단계에 걸쳐 검증하였다. 첫번째로, 자석의 자속밀도를 측정하고 유한요소해석 시뮬레이션과 비교하였다. 두번째로, 방사선 조사된 발치 치아에서 전자상자성공명 스펙트럼을 획득하는 기초 테스트를 수행하였다. 여기에는 220 kVp 에너지 X-선으로 5 Gy와 30 Gy를 조사한 온전한 인간 중절치 두 개가 사용되었다. 마지막 검증 테스트로, 방사선치료 후 환자의 치아를 체내 측정하여 선량을 평가하였다. 이를 위해 사전에 Q 여러 Q 팩터에 대한 선량-반응 곡선을 얻었다. 이 선량-반응 정보를 수집하는 과정에서 앞서 언급한 의사 체내 팬텀이 사용되었다. 온전한 인간 중절치 4개로부터 선량-반응 곡선을 얻었다. 이 선량-반응 정보로부터, Q 팩터와 선량 민감도 및 배경신호의 관계를 획득할 수 있었으며, 이로부터 환자의 Q 팩터에 맞춰 환자 맞춤 선량-반응 곡선이 생성되었다. 이 맞춤 선량-반응 곡선을 기반으로 환자가 치료 중

조사된 선량을 평가하였다.

주요어: 전자상자성공명, 체내 선량평가, 전자상자성공명 치아 선량평가, 의사 체내 팬텀, Q 인자 가변, 전신방사선조사 치료